NICMOS IMAGING OF THE HOST GALAXIES OF $Z \sim 2 - 3$ RADIO-QUIET QUASARS[1]

Susan E. Ridgway and Timothy M. Heckman
Johns Hopkins University, Dept. of Physics and Astronomy, 3400 N. Charles St. Baltimore MD 21218
E-mail:ridgway@pha.jhu.edu and heckman@pha.jhu.edu
Daniela Calzetti
Space Telescope Science Institute, 3700 San Martin Dr., Baltimore, MD 21218
E-mail:calzetti@stsci.edu
Matthew Lehnert
MPE, Postfach 1603, D-85740 Garching, Germany
E-mail:mlehnert@qso.mpe-garching.mpg.de
To appear in the Astrophysical Journal, March 2001

ABSTRACT

We have made a deep NICMOS imaging study of a sample of 5 $z \sim 2 - 3$ radio-quiet quasars with low absolute nuclear luminosities, and we have detected apparent host galaxies in all of these. Most of the hosts have luminosities approximately equal to present-day L_*, with a range from 0.2 L_* to about 4 L_*. These host galaxies have magnitudes and sizes consistent with those of the Lyman break galaxies at similar redshifts and at similar rest wavelengths, but are about two magnitudes fainter than high-z powerful radio galaxies. The hosts of our high-z sample are comparable to or less luminous than the hosts of the low-z radio-quiet quasars with similar nuclear absolute magnitudes. However, the high z galaxies are more compact than the hosts of the low z quasars, and probably have only $10 - 20\%$ of the stellar mass of their low-z counterparts. In one host, we find a residual component that is not centered on the quasar nucleus, and several hosts have apparent companions within a projected distance of ~ 10 kpc, indications that these systems are possibly in some phase of a merger process. Application of the M_{bulge}/M_{BH} relation found for present-day spheroids to the stellar masses implied for the high z host galaxies would indicate that they contain black holes with masses around 10^8 $M_\odot$. Comparison to their nuclear magnitudes implies accretion rates that are near or at the Eddington limit. Although these high z hosts already contain supermassive black holes, the galaxies will need to grow significantly to evolve into present-day L_* galaxies. These results are basically consistent with theoretical predictions for the hierarchical buildup of the galaxy host and its relation to the central supermassive black hole.

Subject headings: galaxies: active — galaxies: evolution — galaxies: formation — galaxies: nuclei — quasars: general

1. INTRODUCTION

Radio-quiet quasars (RQQ) represent the great majority of the known active galactic nuclei (AGN) at high redshift ($z \gtrsim 1$), yet information on the galaxies that host these AGN is currently extremely limited. At lower redshift, luminous RQQ are found in both spiral and elliptical hosts, with the most luminous radio-quiets appearing in the bulge-dominated systems. The host galaxy luminosities correspond to a few times a present-day L_* galaxy (e.g. Bahcall et al. 1997; McLure et al. 1999). In addition, the luminosity of the host seems to correlate roughly with that of the nucleus (McLeod & Rieke 1995; Hooper et al. 1997; McLure et al. 1999; McLeod, Rieke, & Storrie-Lombardi 1999). Nearby, almost every bulge-dominated galaxy may contain a supermassive black hole candidate whose mass is roughly proportional to the luminosity of its bulge (Kormendy & Richstone 1996; Magorrian et al. 1998; van der Marel 1999). The black hole masses are even better correlated with the stellar velocity dispersions observed in the bulges (Ferrarese & Merritt 2000; Gebhardt et al. 2000a). These relationships imply a close correlation between the mass of the stellar bulges in these systems and the masses of their resident black holes.

The evolution in the star formation rate from an epoch of $z \sim 2$ to the present day may be qualitatively similar to the huge drop in the number density of quasars from the peak at $z \sim 2 - 3$ to the present epoch, which is roughly similar to the evolution in the comoving number density of radio sources (e.g, Dunlop 1998; Boyle & Terlevich 1997). All of these factors suggest a strong link between the formation and evolution of galaxies and those of the quasars and their hosts, and support the idea that an active quasar may be a short-lived episode in the life of every bulge-dominated galaxy.

Kauffmann & Haehnelt (2000) have investigated the evolution of the hosts of the radio-quiet quasars and the formation and fuelling of their central black holes using semi-analytic hierarchical clustering models of galaxy formation, and have made specific predictions regarding the evolution of this nuclear magnitude–host galaxy luminosity relation. The high-z radio-quiet quasars are far less studied than the radio-loud host galaxy population, and few observations have been made at nuclear luminosities similar to those of the low-z radio-quiet sample.

To study the evolution of the radio-quiet quasar hosts and their relationship to the other samples of high-z galaxies known, we have made HST NICMOS observations of radio-quiet quasar hosts near the epoch of the peak quasar

---

[1] Based on observations made with the NASA/ESA Hubble Space Telescope, obtained at the Space Telescope Science Institute, which is operated by the Association of Universities for Research in Astronomy, Inc., under NASA contract NAS 5-26555.

density ($z \sim 2 - 3$). We have chosen a sample of quasars whose nuclei are faint enough to provide a good comparison sample to those of the well-studied low-z quasars. Throughout this paper we use $H_0 = 50$ km s^{-1} Mpc^{-1} and $\Omega = 1$, unless otherwise stated.

2. OBSERVATIONS AND DATA REDUCTION

2.1. *Sample Selection*

We have selected 5 quasars with B>21.5 at $z \sim 2$–3 from the faint quasar sample of Zitelli et al. (1992), which is a spectroscopically-complete subsample from the deep optical quasar survey of Marano, Zamorani & Zitelli (1988). The exact redshift ranges were constrained to avoid strong emission lines falling in the NICMOS filter bandpasses near 1.6 μm; this resulted in a sample of 3 objects at $z \sim 1.8$ and 2 objects at $z \sim 2.7$. Their nuclear magnitudes are in the range M$_B$ = -22 to -24, making them comparable in absolute magnitude to many low-z quasar samples (e.g. Bahcall et al. 1997; McLure et al. 1999; McLeod et al. 1999). One object, MZZ 9592, is a BAL QSO (Zitelli et al. 1992).

2.2. *Observations*

The observations were made using the NIC2 aperture of HST's NICMOS camera, which has a field size of 19$''$.2 × 19$''$.2, at a scale of 0$''$.075 pixel^{-1}. To achieve emission-line-free imaging, the $z \sim 1.8$ objects were imaged in the F165M filter, resulting in a rest-frame wavelength of $\sim$V, and the $z \sim 2.7$ objects in the F160W filter, corresponding to rest-frame $\sim$B. To convert count rates into fluxes in Jy, we have used for each filter the HST-supplied calibration factors, i.e. 1 count s^{-1} is 2.07 μJy for F160W and 4.07 μJy for F165M. Where we have used B, V, R, or H-band magnitudes, we have used zero points of 4260, 3540, 2870 and 980 Jy respectively.

We observed each of the 5 quasars (and its corresponding PSF star) with two visits separated by several months, resulting in observations of each field at significantly different position angles on the sky relative to the PSF pattern (which is fixed in the spacecraft frame). This allows an independent check on the reality of any residual emission seen. We used a dither pattern with offsets of $\sim$3$''$ (40 pixels) between integrations, for 6 or 8 integrations per visit. The dither pattern (suggested to us by M. Dickinson, priv. comm. 1997) included half-pixel offsets to improve resolution by adequately sampling the HST PSF at these wavelengths. The final FWHMs achieved were 0$''$.14 – 0$''$.16. We chose a nearby star for each of the 5 quasars, and observed this star in the same visit as the quasar using the identical dither pattern in order to characterize the point spread function (PSF). We imaged in the MULTIACCUM read mode with (primarily) the STEP128 sample sequence for the quasar integrations, resulting in observing times per frame of $\sim$ 900 – 1500 s for the quasars, and 6 – 15 s for their PSF stars. Total exposure times for the quasars were 6000 – 10000 s per visit. However, due to variable cosmic ray persistence problems induced by SAA passages in some of the exposures, the amount of useful data varied from visit to visit. The sky noise levels in the final images therefore differ. We give the summed integration times of data actually used in the final images in the log of observations in Table 1.

2.3. *Calibration*

We recalibrated the raw NICMOS data using a modified version of the standard pipeline process. After identifying the most up-to-date calibration files, we used the STSDAS task *calnica* in a first pass to make basic corrections for the bias and dark contributions, and the non-linearity of the device. We also applied the "CRIDCALC" algorithm which adds the multiple reads and removes the worst of the cosmic rays.

The primary bias anomalies we encountered in our data were the readout artifacts termed "bars", the bias gradients termed "shading" and the variable quadrant bias called the "pedestal effect", described in Skinner et al. (1998) and the NICMOS Data Handbook v. 4.0 (December 1999). We masked by hand any bars that were not removed by the *calnica* routine. To remove the quadrant-dependent pedestal from the frames before flat-fielding, we used the technique developed by Mark Dickinson: his script *pedsky* and the non-interactive version of *pedsky* called *azped2* written by Andrew Zirm and Mark Dickinson. This method works by determining the best value for the sky signal plus quadrant-dependent constant offsets (pedestals) by subtracting various scaled versions of the flatfield, removing an estimated residual bias for each quadrant in this subtracted image, filtering out objects with a median smoothing, then calculating the RMS for the image. The sky value and pedestal values that yield the minimum noise are adopted. This method works well at improving the final flatfielded images for our fairly empty fields. The vertical bands caused by the bias "shading" effect were removed by using the IRAF routine *background* to fit constant values to the columns.

2.4. *Removal of persistent cosmic rays*

The resultant images still vary greatly in quality and depth; this is primarily the result of cosmic ray (CR) persistence after a passage through the South Atlantic Anomaly (SAA). The nature of this problem is more fully discussed in Najita, Dickinson & Holfeltz (1998). Cosmic ray hits during these passages leave residual signal on the detector that decays with time. In our data, depending on the depth of the SAA passage, this residual noise signal can quadruple the effective sky noise and greatly affect the usefulness of specific frames. In many cases, half or more of the sky area is affected by persistent ghosts of CRs. In very severe examples, the frames were saturated by the CR bombardment, and the residual signal takes on a characteristic large scale shape which is correlated to detector properties rather than to the actual location of the hits. In such images, specific spatial masking of the CRs is impossible.

Visits in which CR persistence was a severe problem generally had observations taken in pairs after each SAA passage, with the first much more heavily affected by the CR persistence, and the second carrying the same signal, but at a faded, lower intensity. We can therefore use the frames which have the strongest signature of the SAA passage to remove some of the faded CR signal from the subsequent frame, and therefore greatly decrease the artificial non-Gaussian noise in those frames. We created an object

mask from a combined frame, and used this object mask to mask out the objects in the badly impacted frames, leaving the background. We then subtracted this background-only frame (multiplied by the appropriate scaling factor) from the subsequent frame to remove the persistent CR signal. We used a routine written by Eddie Bergeron to determine the best scaling factor by minimizing the noise in the sky histogram of the difference frame. In many frames this resulted in a $20 - 40\%$ decrease in the effective noise, and resulted in much flatter frames. We then excluded the severely-impacted frames used to model the CR-persistent pattern from the final combination of data.

In general, PSF star observations and object observations were calibrated identically. Of course, because of the relatively short exposure times, CR persistence was not a problem for the PSF star observations.

2.5. *Combination of the data*

Since we have two visits to each object which are at different position angles on the sky, we combine and PSF-subtract each of the two visits to each object separately. This allows us to compare two independent determinations of the fluxes and positions of features in the residual hosts. To determine the relative linear shifts between dither positions, we have calculated centering both from the objects on the frames and from the spacecraft jitter files (where this information was complete), and found no significant difference in result. We then combined the frames, using a simple method that uses the STSDAS routine CRREJ to determine the locations of the CR affected pixels in the initial frames and creates bad pixel masks, resamples the corrected frames to double the linear dimensions, and combines these using standard rejection techniques. The visits that are most affected by the SAA passages may have the number of individual frames reduced to as few as 3, giving the combined image a resolution ~10% worse Use of the "drizzle" technique to shrink the output pixels did not significantly improve the final resolution for our data, probably because we had a limited number of sky positions and the HST PSF at 1.6μm is not severely undersampled by NIC2.

3. DATA ANALYSIS

3.1. *PSF subtraction*

We have made a simple, direct two-dimensional PSF subtraction for each visit on a quasar through an iterative method. We fit a flat background in the combined frame by calculating the mean sky value in an annulus around the quasar that excludes nearby companion objects and most extended flux (generally from about $1\rlap{.}''5$ to $3''$). We centroid the PSF and quasar within a central radius of $0\rlap{.}''09$, and scale the PSF flux to the quasar flux in this aperture. We then vary the centering of the PSF, subtract the two images, and minimize the χ^2 of the residuals to determine the best center. Finding the best relative center is unambiguous since off-center subtractions are obvious in the residuals, and we can treat the scaling and centering independently. Finding the best scaling is more subjective. We would like the residual "host galaxy" to have properties like a real galaxy, and at the least to have a radial profile that increases monotonically. The simplest

way of ensuring this in two dimensions is to require flatness of the residual across some central region. We vary the PSF-quasar scaling of the subtraction until the mean value in the residual of an annulus (from $0\rlap{.}''09 - 0\rlap{.}''15$) is equal to that of the inner $0\rlap{.}''09$ aperture. This method is discussed further in Ridgway & Stockton (1997). This will still likely result in an oversubtraction, depending on how peaked the real host galaxy is within this inner radius. If there is no significant excess flux in the outer annulus, the PSF-quasar scaling determined will be equivalent to the most conservative limit of subtracting the central region to zero residual flux.

We achieved the cleanest subtraction with the PSF star observed during the same visit as the quasar; for one visit of MZZ 1558, we were unable to obtain a PSF star, and we have used the PSF star from the other visit without major problems. The count rates in the observed PSF stars are in all cases thousands of times greater than those of the quasars and therefore signal-to-noise in the PSFs was not a concern. The scaling factors (QSO/PSF) range from 10^{-3} to 10^{-5} for the PSF stars; the MZZ9592 quasar-to-field-star ratio is 0.26. The PSF scaling factors differed by $<1\%$ up to 8% between the two visits for each object.

As a result of this subtraction process, we find resolved excess two-dimensional flux around the quasars relative to the PSF stars, in each of the two visits to each quasar. The quasar hosts are also resolved relative to a star with an apparent magnitude similar to those of the quasars that fell within the field of MZZ 9592. This field star provides a good check that our results are not the product of some difference in the way we have observed and reduced the PSF stars versus the quasars. We have thus also treated this star as if it were a quasar and applied the same PSF subtraction techniques to it; we find no significant flux in the residual.

In Figure 1, we show the results of these analyses for both visits to MZZ 9592, separately. The extension around MZZ 9592 consists of a bright, relatively symmetric halo of emission relative to both the PSF and the field star, but has in addition an off-nuclear component which will allow us to check that our resolved morphology is stable. This component appears at the same location in both visits and regardless of whether the field star or the observed PSF star is used for subtraction. Results of aperture photometry of the residual are consistent within a few percent for each visit and subtraction variation. These tests show that our results are not likely to be an artifact of our observing or analysis method.

3.2. *PSF-subtracted host galaxy images*

To create the best S:N image of the extended host, we combine the PSF-subtracted images from the two visits by centering using the quasar, rotating using the nominal sky position angle (ORIENT header parameter), and averaging, after weighting the two visits by the inverse variance of the sky noise.

In Figures 2 and 3, we give these PSF-subtracted combined results for the 5 quasars, both at the original resolution and smoothed with a Gaussian kernel with $\sigma = 0\rlap{.}''06$. In each of the five quasars we detect extended flux around the quasar nucleus. The faintest residual is that of MZZ 4935, whose extended residual we detect at about the 3σ

level.

The PSF-residuals create the noisy, ringing patterns seen in the central regions of the images, with a radial extent that varies slightly depending on the brightness of the quasar nucleus and details of the PSF observations. The noisy regions are mostly $<0\rlap{.}''15$ in radius. For MZZ 1558, however, we did not have a PSF star from the same visit for one of our observations, and this PSF–quasar fit is not as good, resulting in obvious subtraction residuals to a larger radial extent. In all cases, however, we detect flux outside of these noisy inner regions.

3.3. *One-dimensional enclosed flux and radial profile plots*

Another direct way of presenting the difference between the PSF stars and the quasars is by comparing radial plots of the enclosed cumulative flux, providing a one-dimensional, azimuthally-averaged view of the excess flux. We show in Figure 4 the results of making this analysis for both observations of the quasar MZZ 9592, and for both observations of the available comparison stars: the primary bright PSF star, a secondary bright PSF which fell off-center but within the PSF star field, and the field star of comparable brightness to the quasar which fell on the quasar field. The enclosed flux at each radius is normalized to that found within a radius of $0\rlap{.}''075$, which corresponds to a diameter of ≈ 1 FWHM. The two quasar enclosed flux profiles deviate significantly from all of the stellar enclosed flux profiles, despite some variation in both quasar and PSF profile from observation to observation.

We display in Figure 5 the enclosed flux profiles for the rest of the quasars and their corresponding PSF stars (in these cases, averaged over the two observations). The plots are once again normalized such that the quasar and PSF have the same total flux of 1 within a radius of $0\rlap{.}''075$.

We see in Figs. 4 and 5 that the 5 quasars all deviate positively from their PSF stars (having more enclosed flux) within the inner $1''$ radius, and that most of the excess flux is within this radius. Companion objects are also visible in these plots.

To better inspect the radial behavior of the difference between the quasar and PSF profiles, we have also made radial profile plots of the mean surface brightness of the final PSF-subtracted quasar residuals. These are shown in Figure 6 for the 5 quasars. The mean surface brightnesses are calculated in bins of $0\rlap{.}''019$, and we show in each case a statistical error for the contribution of sky noise to the average bin. However, the noise between bins is highly correlated in these resampled, smoothed images.

These plots show clearly the spatial extent of the azimuthally averaged residual hosts; i.e., most flux that is not a discrete apparent companion object is contained within the inner $1''$ radius.

4. RESULTS

4.1. *Photometry*

To provide the simplest basis for cross-comparison between samples, we have first calculated simple aperture magnitudes. We have used apertures with radii ranging from $0\rlap{.}''22$ to $1\rlap{.}''4$ and quote the values from the $0\rlap{.}''6$ and $1\rlap{.}''0$ radius apertures. As these extensions are mostly fairly compact, the smaller aperture includes most of the flux

and reduces sky noise, while the larger aperture, corresponding to an average diameter of ~16 kpc at these redshifts, still excludes most nearby discrete companions and is more useful for comparison to other samples of objects. To estimate errors, we have also calculated the host magnitudes for the two visits separately. Though the quasar is resolved in each of the two visits in all cases, for those objects in which the hosts are smallest in size (e.g. MZZ 9744) or faintest (MZZ 4935) the flux of the residual varies between the two visits more ($\sim40\%$) than in those cases where the host is bright and extended (e.g. MZZ 9592, visit-to-visit difference $<5\%$). We include these differences in our estimates of the errors in our quoted magnitudes.

The results of our magnitude analysis for these two apertures is given in Table 2, and in Table 4 are the fluxes and absolute magnitudes of the quasar nuclei alone. The detected hosts vary from less than L_* to 4 L_*, using L_*^V and L_*^B at $z = 0$ from the field galaxy luminosity function of Loveday et al. (1992), i.e. $M_B^* = -21.0$, and for colors of a Sa, $M_V^* = -21.8$. The errors given are generally from the systematic variation seen between the two visits or estimated from obvious uncertainties in the subtraction, although in a few cases the sky noise in the aperture was greater (e.g. MZZ 9592). The faintest residual host (around MZZ 4935) we detect at a flux $\sim0.2L_*$, and is best detected in the first visit which was less affected by persistent CR problems. This aperture flux corresponds to a 3σ detection in the $1\rlap{.}''3$ diameter aperture, where the 1σ noise was determined by measuring the irregular background fluctuations in the sky of the combined frame.

These fluxes need a correction for flux lost from the PSF subtraction process which will vary depending on how compact the intrinsic, underlying host is. In Section 5 we discuss simple models to estimate the amount of this correction.

4.2. *Morphologies*

The morphologies of these hosts are quite compact, as demonstrated by our aperture photometry in that most of the flux is contained within a $0\rlap{.}''6$ radius aperture. A simple way of quantifying the morphologies of these hosts is to determine the half-light radii ($r_{\frac{1}{2}}$), the radius at which half the flux is enclosed for each residual host. We use as the total flux the flux enclosed within a $1''$ radius. Inspection of the enclosed flux in the residuals as a function of radius for each object shows a flattening of the enclosed energy profiles at radii of $0\rlap{.}''6 - 1''$, before contributions from nearby companions. (MZZ 9744 has a discrete companion at $0\rlap{.}''8$, and excluding this companion has no significant effect on the scale size derived). These "direct" $r_{\frac{1}{2}}$ values are in column (3) of Table 3. By making these estimates of the half-light radii we have essentially assumed that the flux profile within the inner $0\rlap{.}''2$ radius is flat, and these values may therefore be overestimates if the flux profile is more sharply peaked. Statistical error in the enclosed flux results in only a small statistical error in $r_{\frac{1}{2}}$, $\sim0\rlap{.}''02$, but systematic errors caused by assumptions about the profile and errors in PSF subtraction may be greater.

In addition, we make fits to the azimuthally-averaged radial profiles of the two brightest residual hosts, using simple 1D exponential disk and de Vaucouleurs profile models

to extrapolate the central $0\rlap{.}''2$ radial region. The half-light radii resulting from these fits are in column (4) of Table 3 for MZZ 9592 and MZZ 11408, in which the residual hosts are least affected by the PSF subtraction process. (For the de Vaucouleurs profile, $r_{\frac{1}{2}}$ is equal to the effective radius r_e, while for the exponential disk model, $r_{\frac{1}{2}}$ is 1.6783 times the exponential scale length.) The fits were made in the radial region $0\rlap{.}''23 < r < 1\rlap{.}''2$ to exclude the inner PSF-dominated disk, and reduce sky noise. The range in scale sizes quoted are a result of varying slightly the fitting radial regions while still maintaining a reasonable fit. These fits are intended as a cross-check on the validity of the direct $r_{\frac{1}{2}}$ derivations, and the results are consistent.

The scale sizes (from all methods) are securely less than $\sim 0\rlap{.}''5$ (~ 4 kpc), and the mean scale size based on the direct $r_{\frac{1}{2}}$ determinations is ~ 2.3 kpc in physical scale.

In two cases (MZZ 1558 and MZZ 9744), there are galaxies close to the quasar in projection ($\lesssim 10$ kpc), and in one (MZZ 9592) there is an off-center component in the residual host. In MZZ 1558, at $z = 1.829$, the companion galaxy is at a projected distance of $1\rlap{.}''3$ (11 kpc) from the quasar, and has a $1\rlap{.}''3$ aperture flux of 2.2 μJy, while the quasar host itself has a flux of 10% less. This could therefore be an example of an early stage of an equal mass merger. In the case of MZZ 9744, the nearest companion in projection is of much less flux than the host. Assuming these companion galaxies and residual component are associated, some of these hosts may not be completely relaxed systems, and could be in some stage of a merger. However, other than these fairly discrete apparent companions and residual component, the hosts appear regular. After subtraction of a regular 2D galaxy model from the two brightest hosts, the off-center component in MZZ 9592 is more visible and appears compact; in contrast, a similar subtraction from MZZ 11408 leaves no irregular components (Fig. 7).

5. COMPARISON TO OTHER SAMPLES OF GALAXIES: SIMULATIONS

In order to compare this sample of galaxies to other samples of observed high-z galaxies, we need to understand how the presence of the quasar nucleus and the PSF-subtraction procedures as well as the observational parameters (such as exposure time and resultant sky noise) affect our ability to measure the magnitudes and morphologies of the hosts. The simplest way of addressing this issue is to simulate our quasars with other observed galaxies, as well as noiseless models.

5.1. *Quasar simulations with NICMOS-observed HDF-N Lyman break galaxies*

We have made some simple simulations of the effect the presence of the quasar nucleus and the PSF-subtraction process have on the derived magnitudes and morphologies. We have used for the first set of these simulations a sample of spectroscopically-identified $z \sim 2 - 3$ Lyman break galaxies (LBGs) from the HDF North (Dickinson 2000). We were kindly provided with the drizzled, calibrated NICMOS image by Dickinson et al. (2000). This NIC3 F160W image was observed to a much greater depth than our observations.

We made "artificial quasars" at two fiducial redshifts, $z = 1.8$ and $z = 2.7$, to simulate our observed data. To do this, we used cutout images of the Lyman break galaxies in this sample that are within about 0.3 redshift units of these two redshifts, and correct their fluxes and scale sizes for cosmological effects, giving us a sample of 12 objects for the $z = 2.7$ models, and 6 objects for the $z = 1.8$ models. After resampling these imaging data to match our pixel scale, we added to the galaxy center nuclei of varying magnitudes (matching the range of magnitudes observed), using the MZZ 9592 field star as the nucleus. (We also ran a set of simulations using a selection of observed PSF stars as the nuclei). Background and Poissonian noise were added to match the average noise seen in the observed quasar images, with the limiting surface brightnesses normalized to the model redshifts of $z = 1.8$ and $z = 2.7$.

After running a standard PSF-subtraction using the PSF star observed in the same visit as the field star, we have calculated the flux in the same apertures used for the real quasars, both in the PSF-subtracted simulated quasar and the original galaxy used for each model. In Figure 8, we show a few examples of HDF Lyman break galaxies before and after the modelling process. In Figure 9 we show the results of the photometry of the $z = 1.8$ and $z = 2.7$ model samples. The success of the process in recovering the input flux of the galaxy varies with the flux and scale size of the original galaxy, and with the effective brightness of the overlying quasar. We give the input parameters of the models and the resultant Δ magnitudes in Table 5, where we also indicate which model is simulating which of our 5 quasars. From inspection of these simple models, we find first, that the bulk of the flux offset occurs in the central $0\rlap{.}''5$ diameter section; second, that the addition of the noise and the specifics of the PSF – nucleus profile mismatches can cause small offsets in the flux either way, although the trend for most models with peaked galaxies is for the subtraction process to decrease the flux. In addition, the brighter the overlying nucleus, the larger the decrease in the derived flux.

In the plots shown here, we used the MZZ field star as the "nucleus" of the model quasar and the observed PSF star from the same visit as the subtraction PSF, which should be the most representative of an observed quasar nucleus/PSF star pair. Using the various PSFs as the nuclei and subtracting other PSFs from different visits gave results with similar trends, but with more scatter, as the PSF residuals are significantly larger if they are not observed in the same orbit.

5.2. *Quasar simulations with observed radio galaxies*

We have also made equivalent models with some NICMOS F160W and F165M images of powerful radio galaxies at $z = 2 - 3$ (Pentericci et al. 2000; Pentericci 2000) selected primarily from the MRC sample of McCarthy et al. (1996). Taking from their sample only the observations of galaxies that are completely emission line-free and resolved would limit us to only two objects. We have also therefore included galaxies that have relaxed elliptical morphologies; these galaxies are less likely to have major contributions from extended emission-line regions. The final sample comprises 4 $z \sim 2$ and 3 $z \sim 3$ radio galaxies.

We apply to this sample the same modelling process described in 5.1, A few examples of the results are shown in Fig. 10; in essence, this is how a few typical powerful radio galaxies at $z \sim 1.8$ and $z \sim 2.7$ would appear had they contained quasar nuclei similar to those of our quasars and had been observed to almost the same depth. In some of these radio galaxies (as discussed in Pentericci et al. 2000) there is a large intrinsic contribution from unresolved nuclei; this unresolved nuclear component is removed by the subtraction process and results in a large change in magnitude. As can be seen from Table 5, the Δ magnitudes are larger than for the Lyman break galaxies, ~ 0.3 and 0.4 mags for the $z = 1.8$ and $z = 2.7$ models.

5.3. *Comparison to low-z quasars: bulges and disks*

In order to make a good comparison of the high-z quasar hosts to the well-studied low-z quasar hosts, we have made another set of simulations. In this case, we wished to estimate how a typical low-z quasar host would appear at $z = 1.8$ and $z = 2.7$, with nuclei of comparable brightnesses to ours and imaged under similar observational conditions. From these simulations we can also determine whether our seemingly compact, moderate-luminosity hosts could simply be the tips of typical, larger scale-size elliptical or disk galaxies, in which most of each galaxy has been obscured by sky noise.

Bahcall et al. (1997) and McLure et al. (1999) both have imaged samples of low-z ($z \sim 0.2$) quasars with WFPC2 at $\sim R$-band, giving absolute magnitudes and scale sizes of the hosts at close to rest-frame V, similar to the rest-frame of our high-z H band observations. We therefore convert Bahcall et al.'s total absolute V magnitudes (from their Table 12) to our cosmology, and their scale sizes for fitted disk and bulge models to half-light radii, and find that their average (of 14) radio-quiet quasar hosts has an absolute V magnitude $M_V = -22.1$, with a 1σ variation of 0.6. The average $r_{\frac{1}{2}}$ is 8.1 kpc. We have also used the total R magnitudes for the radio-quiet quasar sample of McLure et al. (1999) (from their Table 2). We converted these to M_V and found the average RQQ host to have $M_V = -22.7$ with 0.6 mag variation, and half-light radius of 8.2 kpc (if one host with $r_{\frac{1}{2}} = 23$ kpc is excluded). For our models, therefore, we have adopted a $r_{\frac{1}{2}} = 8.2$ kpc as typical, and have used both $M_V = -22.1$ and -22.7 for a reasonable spread in brightnesses.

We generated noiseless galaxy models with both $r^{\frac{1}{4}}$-law and exponential disk radial profiles with half-light radii of 8.2 kpc, which corresponds to $0\rlap{.}''98$ and $0\rlap{.}''92$ at $z = 1.8$ and $z = 2.7$ respectively. After scaling the model hosts to the appropriate apparent magnitudes and making the slight necessary K-corrections, we convolved the model galaxies with the seeing disk of our observed PSFs, and simulated the observed quasars in the same way described in the previous sections. In Figure 11 are shown a few examples of the resultant images, all for the fainter absolute host magnitude ($M_V = -22.1$). In terms of the amount of flux recovered, the disk model galaxies fare slightly better than the ellipticals, but the difference is minor. The Δ magnitudes given in Table 5 are therefore averaged over the model types and brightnesses. The total host flux lost is not significant ($\sim 0.1 - 0.2$ mags) at $z = 1.8$, though is worse for the brighter nuclei at $z = 2.7$ ($\sim 0.3 - 0.4$ mags).

To estimate how much our scale size determinations could be affected by the PSF-subtraction and and sky noise, we have also made 1D azimuthal averages of the model galaxies before and after the modelling process, and attempted to fit these residual profiles directly. We find that the fitting is not always stable, but most of the fitting to the residuals reflects accurately the relatively large scale sizes of the input models. In the worst case, however, of the fainter elliptical host at $z = 2.7$ with the brightest of the model nuclei, we did find incorrect, compact scale sizes. This is the model shown to the far right of Figure 11 in which 1D residual fits found a half-light radius of $\sim 0\rlap{.}''2$. In this case, too much of the extended material has been lost to sky noise to make an accurate determination of the original scale size from the residual. However, except for the highest redshift objects with the brightest nuclei, these models indicate that we can probably differentiate the compact MZZ hosts easily from a noisy host galaxy with larger scale size. The smoothness of the input host model accentuates this problem, and determinations of scale sizes in the Lyman break simulations were more successful.

5.4. *Aperture and subtraction corrections*

To estimate the total magnitudes in our hosts we make two corrections to our aperture magnitudes: a "subtraction" correction, to estimate the amount of flux lost to the PSF subtraction process, and a simple aperture correction, for the amount of flux that will lie outside our aperture.

The subtraction correction is the greater source of uncertainty, and will depend strongly on how compact the inner regions of the underlying galaxy are, and on the brightness of the overlying quasar nucleus. We have summarized the decrements in host magnitude that resulted from our various simulations in Table 5, as a function of galaxy type, galaxy redshift, and quasar nuclear magnitude. The Lyman-break galaxies are compact and faint, and of the three types of galaxies (LBGs, radio galaxies, and low-z quasar hosts) modelled, are the most comparable to the MZZ hosts. We therefore use as the subtraction correction for each host the average Δ magnitude found from the LBG models. The quasar name and the corresponding Δ magnitude used are found in columns (4) and (5) respectively of Table 5.

For the aperture corrections, we have assumed that our host galaxies are pure disks or ellipticals with the scale sizes we have determined from the residuals, and have estimated the amount of flux that lies outside of our standard $2''$ apertures. The scale sizes were primarily in the range of $0\rlap{.}''2 - 0\rlap{.}''4$. The corresponding range in magnitude corrections for the elliptical models are 0.14 – 0.39 mags for the $2''$ aperture. For the disk models, the magnitude corrections necessary are smaller, with a range of 0.0 – 0.18 mags for the $2''$ aperture. We quote in column (5) of Table 3 the aperture corrections we adopted for each quasar.

From a combination of these subtraction and aperture effects, we estimate a probable correction from the $2''$ aperture to a total magnitude for each host, and give this corrected "total" magnitude in the last column of Table 2.

6. DISCUSSION

We have detected host galaxies around all five of our sample of $z \sim 2 - 3$ radio-quiet quasars. The detected hosts have absolute V magnitude $M_V \sim -20.2$ to -22.5, with absolute luminosities from less than present-day L_* to $4\,L_*$. The quasar nuclei are of relatively faint absolute B magnitudes, with M_B ranging from -24 to -22. The scale sizes, where we can fit the residuals, yield half-light radii of <4 kpc.

6.1. *Host galaxy magnitudes compared*

Observational resolution is obviously important in studying the hosts of quasars, particularly those at high redshift, since (at $z = 2$) ~ 8 kpc of physical scale would be hidden under a typical $1''$-diameter groundbased seeing disk. We will thus compare our work primarily to the results of other HST imaging; however, work has been done on high-z quasars with ground-based resolution that provides tantalizing hints of possible correlations. While Lehnert et al. (1992) found bright hosts around 6 $z \sim 2.5$ radio-loud quasars in ground-based near IR imaging, Lowenthal et al. (1995) detected no hosts around a comparison sample of RQQ at the same z and nuclear magnitudes. This result implied that the host luminosity might correlate with radio-loudness. In contrast, Aretxaga et al. (1995, 1998) studied several very luminous $z \sim 2$ RQQs and found hosts comparable in luminosity to those found in the RLQ sample of Lehnert et al. (1992), indicating perhaps a heavy dependence of host magnitude on the nuclear luminosity.

Our observations of the $z \sim 2 - 3$ RQQ sample benefit from the compact and stable NICMOS PSF. Indeed, our simple simulations with observations of other high-z galaxies have indicated that for most intrinsic galaxy morphologies our estimates of the magnitudes and morphologies are not badly affected by the presence of the quasar nucleus and observing process.

We have quoted in Table 2 simple aperture magnitudes, with error estimates based on the variation in the subtraction and from the sky noise. In the last column, we also give a rough estimate of "total" magnitude, based on adding the systematic subtraction and aperture corrections discussed in section 5.4 to the $2''$ aperture magnitudes. It is these estimates of total magnitude that we will use in comparing our host galaxy properties to those of other samples of galaxies.

We plot in Fig. 12, for two different cosmologies, the absolute rest-frame V total magnitudes of the 5 MZZ quasar hosts, extrapolating our $z \sim 2.7$ quasar host M_B values to M_V assuming the hosts have a spectral index of -2 (i.e. flat in F_λ), corresponding to a $(B-V)$ of 0.7.

We also correct to rest-frame M_V and plot on these figures the Lyman break galaxy magnitudes from the Dickinson (2000) sample, the powerful MRC/USS radio galaxies of the Pentericci et al. (2000) sample, and at low-z, the quasar host magnitudes from the Bahcall et al. (1997) and McLure et al. (1999) samples. In addition, Lacy et al. (2000) have made ground-based K' imaging studies of a $z \sim 2 - 3$ sample of faint 7C-III radio galaxies for which we have both small and large aperture magnitudes, and we have included these as well.

We have used in all cases simple estimates of total magnitudes, applying corrections to the available aperture

magnitudes of generally less than 0.3 mags. For the HDF LBG galaxies, we measured the magnitudes directly from the image provided by Dickinson et al. (2000). As these galaxies have similar compactness to our host galaxies, we used the same metric apertures used for our quasar hosts (i.e. $2''$ at $z = 1.8$ and $z = 2.7$, corresponding to ~ 16 kpc), and made similar aperture corrections to total magnitude as those used for the MZZ quasar hosts. For the Pentericci et al. (2000) bright radio galaxy sample, we have corrected their quoted $4''$ aperture magnitudes to total magnitudes assuming the hosts are ellipticals with scale sizes of 10 kpc (corrections of $\sim$0.25 mags). For the 7C-III radio galaxy sample of Lacy et al. (2000), we correct the quoted 64 kpc aperture magnitudes to total, with the same assumptions (resultant corrections $\sim$0.15 mags). The low-z quasar host magnitudes of Bahcall et al (1997) and McLure et al. (1999) are discussed in more detail in section 5.3, but do not require correction to total magnitude. All magnitudes were observed at close to rest-frame B or V and therefore the K-corrections are minor.

The MZZ quasar host galaxy magnitudes at both z ranges are much more consistent with those of the Lyman break galaxies at high-z than with either sample of radio galaxies. At $z \sim 1.8$, our mean M_V is about -21.5, while the radio galaxies have mean $M_V \sim -24.0$. At higher z, the difference is less, particularly between the less luminous 7C-III galaxies and our hosts, but the means still differ by almost 2 magnitudes. When compared to the Lyman break galaxies, the MZZ hosts span the same range of magnitudes over this redshift range.

Our derived magnitudes are similar to those of the low-z quasars: slightly less luminous in the high Ω_m cosmology, and comparable in the low Ω_m cosmology. However, the stellar masses corresponding to these absolute V magnitudes will be much less for the young, high-redshift galaxies than for the old stellar populations probably associated with the low-z galaxies. We have placed models of the passive evolution of some simple stellar populations on the figures.

These models have been generated with the most recent of the Bruzual & Charlot population synthesis models (Bruzual & Charlot 2000), using a Salpeter IMF and an upper mass cutoff of 100 $M_\odot$, with metallicity $Z = 0.02$ (Charlot 2000, priv. comm; further discussion of these models can be found in Bruzual & Charlot 1993; Liu, Charlot, and Graham, astro-ph/0004367). The dashed line represents a model with an instantaneous burst of star formation at $z = 5$, while the dot-dashed line represents a model with a 1 Gyr burst of star formation ending at $z = 3$. The evolutionary tracks are roughly normalized to the absolute V magnitudes at $z = 1.8$ of (1) the MZZ quasar hosts and 2) the powerful radio galaxies. This corresponds to total masses in *e.g.*, the instantaneous burst model, of (1) 1.1×10^{11} $M_\odot$ (Ω_m=1) or 2.0×10^{11} $M_\odot$ ($\Omega_m = 0.3$) and (2) 1.2×10^{12} $M_\odot$ (Ω_m=1) or 1.9×10^{12} $M_\odot$ ($\Omega_m = 0.3$). The total stellar masses for the 1 Gyr burst models are about $20 - 30\%$ smaller. The degree of fading is about $2.2 - 2.5$ magnitudes in V from $z = 2.7$ to $z \sim 0$ and $1.5 - 1.7$ magnitudes from $z = 1.8$ to $z \sim 0$, for the range of models and cosmologies considered, corresponding to (M/L) increases of ~ 10 from $z = 2.7$ to $z \sim 0$. In other words, at $z = 0.2$, our mean quasar host would be

about 2 magnitudes fainter than the mean $z = 0.2$ quasar host from the McLure et al. and Bahcall et al. samples if it evolved passively from a short burst of star formation at $z = 3 - 5$. This implies that the mean MZZ quasar host may have about one sixth the stellar mass of the mean low-z quasar host.

Thus we find that the hosts of $z \sim 2 - 3$ radio quiet quasars with faint nuclei ($M_B \sim -24$ to -22) have magnitudes that are consistent with their being drawn from the population of Lyman break galaxies observed at similar redshifts.

Our results are consistent with other recent NICMOS results on some brighter, lensed quasars; Rix et al. (1999) find that their sample of lensed $z \sim 2$ radio-quiet quasars (de-magnified $M_B \sim -24$ to -28) had hosts with comparably faint magnitudes. In addition, first results from the large NICMOS quasar host survey of Kukula et al. (2000) have been reported, giving similar or slightly brighter host magnitudes for a sample of 5 $z \sim 2$ RQQs with nuclear $M_B \sim -24$.

These magnitudes are not consistent, however, with those of the sample of radio galaxies at similar redshifts nor with these high-z quasars passively evolving into the hosts of the low-z quasars.

6.2. *Host galaxy morphologies compared*

We also compare the morphologies of our quasar hosts with those of the other samples of high-z objects for which there are good estimates of scale sizes in the rest-frame $\sim V$ or B. Though our determinations of scale sizes are very approximate, in no cases did we find evidence for a half-light radius more than 4 kpc ($\sim 0.''5$ at these redshifts). These scale sizes are more consistent with those of the Lyman break galaxies than with those of the high-z radio galaxies or low-z quasar hosts, and our simulations have strengthened this result.

The $z = 2 - 3$ HDF-N Lyman break galaxies are found to be quite compact in the rest-frame UV WFPC2 imaging, with scale sizes of $\sim 0.''2$–$0.''3$ (Giavalisco et al. 1996; Lowenthal et al. 1997). The NICMOS F160W imaging, most comparable to our studies of the MZZ quasars, revealed similar compactness in the LBG sample, with identical or even more compact half-light radii than those measured in the optical (Dickinson 2000). On the other hand, the low-z quasar hosts are found to have half-light radii of $8 - 15$ kpc in the rest-frame V WFPC2 imaging, consistent with their being relaxed giant ellipticals or evolved disk galaxies (McLure et al. 1999; Bahcall et al. 1997).

Comparison to the morphologies of the high-z radio galaxies is less simple, as there may be some dependence of the half-light radii on the luminosity of the radio sources (e.g. Roche, Eales & Rawlings 1998; Lacy et al. 2000). Generally, however, at $z \lesssim 1.5$, the galaxies (with a range in radio luminosities) are found to be well-fit by $r^{\frac{1}{4}}$ laws, with half-light radii in the range of $5 - 11$ kpc (Roche et al. 1998; Best et al. 1998; McLure & Dunlop 2000; Lacy et al. 2000). Pentericci et al. (2000), however, indicate that the powerful radio galaxies in their sample at $z > 2$ have scale sizes 3 times less than those at $z \sim 1$, while Lacy et al. (2000) find less evolution in scale size. While the best determinations of scale size at rest-frame V are these NICMOS observations of the MRC/USS sample of Penter-

icci et al. (2000), their sample is fairly small and reveals a large range in scale size. In 5 cases, they were able to fit de Vaucouleurs profiles, and determined $r_{\frac{1}{2}}$ values ranging from $0.''2$ to $1.''6$. In Lacy et al. (2000), a summary of the available morphological data in the literature (including the measurements of Pentericci et al.), plus the results of ground-based scale size determinations on the 7C-III sample, indicate that at $z \sim 2 - 3$ the mean scale size of high z radio galaxies is $\sim 0.''6$, with the same large range found in the MRC/USS sample. Thus, although some of the high-z radio galaxies have scale sizes as compact as the LBGs or the MZZ quasar hosts, the mean $z \sim 2$ –3 radio galaxy is probably still more extended.

With such a small number of objects we cannot effectively judge how significantly "disturbed" the morphologies in this sample are in comparison to other samples of high-z galaxies. Three of our 5 quasars have discrete companion objects or a compact component within 10 kpc of the quasar and otherwise seem to have regular morphologies. Overall, this level of "disturbance" in the sample is consistent with the complex morphologies seen in the Lyman break and radio galaxy samples. However, even the low-z quasar hosts have some discrete residual components and tidal tails that are visible after subtraction of the main galaxy component (e.g. McLure et al. 1999), and an unusually high incidence of nearby companions is also noted (Bahcall et al. 1997).

6.3. *Black hole masses, quasar luminosities, and quasar host properties*

We also wish to investigate the relationship between the quasar host properties, the luminosities of the quasar nuclei, and the masses of the nuclear black holes. In particular, a number of results have lent support to the idea that the AGN luminosity and the mass of the host galaxy may be linked. Studies of nearby spheroids indicate that nearly every present-day stellar spheroid contains a massive black hole (BH), and that the masses of the black holes and the luminosities of the bulges (and therefore by inference the masses of the bulges) are linearly correlated (Kormendy & Richstone 1996; Magorrian et al. 1998; van der Marel 1999). The stellar velocity dispersions of these bulges may provide a more direct measure of their masses, as evidenced by the even tighter correlation of velocity dispersion with black hole mass (Ferrarese & Merritt 2000; Gebhardt et al. 2000a). The BH masses determined from this velocity dispersion correlation are consistent with those determined from reverberation mapping of AGN (Gebhardt et al. 2000b). All of these results imply a close link between the formation of the bulges of the galaxies and the formation of the black holes found within them.

If more massive black holes translate into more powerful quasar nuclei, we might then expect that the brighter AGNs (including both brighter radio sources and quasars of greater nuclear luminosity) would have the most luminous and most massive hosts. In fact, there is an upper bound to the luminosity of the low-z quasars that is consistent with Eddington-limited accretion onto supermassive black holes with masses given by the local M_{BH} vs. M_{bulge} relation (McLeod, Rieke, & Storrie-Lombardi 1999; McLure et al. 1999; Laor 1998).

To make an estimate of the masses of the black holes associated with these MZZ quasars, we can apply the local M_{BH} vs. M_{bulge} relation to our host galaxies. We have used the van der Marel (1999) normalization of this relationship, and have made corrections for the much lower M/L ratio at the redshifts of our objects than at $z = 0$ (estimated from the passive evolution models discussed earlier). This results in black hole masses mostly around 1×10^8 M$_\odot$, but ranging from $0.3 - 2 \times 10^8$ M$_\odot$. These values are given in Table 6. We then use these derived black hole masses and the M_B nuclear magnitudes of the quasars to estimate the ratio of the quasar luminosity to the Eddington luminosity, making a bolometric correction to the B band of a factor of 12 (Elvis et al. 1994). We find accretion rates that vary from 0.2 to 1.4 times the Eddington limit, with most at 70% of the Eddington accretion rate (also in Table 6). This is consistent with schemes in which high-z radio-quiet AGN are associated with moderately massive black holes and accrete at close to the Eddington rate, while luminous radio-loud objects are believed to be accreting at sub-Eddington rates and to be associated only with the most massive black holes ($>10^9$ M$_\odot$) (Rawlings & Saunders 1991; McLure et al. 1999; Willot et al. 1999; Lacy, Ridgway & Trentham 2000). In contrast, Rix et al. (1999) found comparable host magnitudes for a much brighter set of quasars, and hence found accretion rates that were super-Eddington.

Another way of estimating the black hole masses in AGN is by using the velocity dispersion of the $H\beta$ emitting clouds in the broad-line region (BLR), (as measured by the $H\beta$ FWHM), in combination with some estimate of the size of the BLR emitting region, and assuming that the dispersion is from virialized cloud motion (e.g. Laor 1998; Wandel et al. 1999). Wandel et al. compare reverberation mapping estimates of the black hole masses in a sample of Seyferts and quasars to estimates from the $H\beta$ FHWM, and found they correlated well. Laor (1998) found that the $H\beta$-derived BH masses in the Bahcall et al. quasar sample correlated well with the black hole masses derived from the Magorrian et al. (1997) M_{bulge} / M_{BH} relation. From the identification spectra for the MZZ quasars (Vitelli et al. 1992), we can estimate very rough CIV FWHMs for 4 of the quasars (in the range 6500 to 7500 km s^{-1}), and use these as representative of the $H\beta$ widths. Laor (1998) estimates the radius of the BLR as proportional to the square root of the bolometric luminosity, and adopting his formulation and our previous estimates of the bolometric nuclear luminosity we find black hole masses for these quasars of about 3 to 8×10^8 M$_\odot$. The derived masses are roughly proportional to those we derived from the van der Marel (1999) relation but are about a factor of 4 larger. However, both Wandel et al. and Laor found that their correlations required separate calibration, and as we have used a different line, and the available spectra are insufficient to make reliable estimates of the line FWHMs, this discrepancy is not surprising.

6.4. *Implications*

Observations of galaxies at high-redshift to date have focussed largely on two very distinct populations: powerful radio-loud AGN (chiefly radio galaxies, but including radio-loud quasars), and normal star-forming galaxies (the Lyman break population). One of the major goals of our investigation is to better understand the relationship of the hosts of typical radio-quiet AGN to these other populations.

We have found that the radio-quiet quasar hosts are similar to the Lyman break galaxies in terms of rest-frame optical luminosities and sizes, but are considerably less luminous and smaller than radio galaxies at similar redshifts. These results have some interesting implications. We will consider the comparisons to the radio-loud AGN hosts first, and then briefly discuss the Lyman break galaxies.

6.4.1. *Evolution of quasar and radio galaxy hosts*

Our results reveal an interesting discrepancy between the evolution of the radio-quiet and radio-loud host galaxies. At low-z, luminous radio-quiet quasars are found primarily in massive early-type galaxies with luminosities of several times a present-day L_* galaxy (e.g. Bahcall et al. 1997; McLure et al. 1999; McLeod et al. 1999), and have properties that are comparable to those of the radio galaxies. McLure et al. have compared carefully selected samples of radio-quiet quasars, radio-loud quasars, and radio galaxies at $z \sim 0.2$ and shown their host properties are all similar (with the radio-loud objects in slightly brighter hosts that those of the radio-quiet). However, despite being nearly indistinguishable from radio galaxy and radio loud-quasar hosts at low z, at high z the radio-quiet quasar hosts are several magnitudes fainter than the radio galaxies.

The cosmic evolution of the population of powerful radio galaxies has been well-documented over the past decade (e.g. Röttgering, Best, & Lehnert 1999). Radio galaxies (over a wide range in radio power) are found in relaxed, massive elliptical hosts up to fairly high redshift ($z \sim 2.5$) and have K magnitudes with low dispersion, consistent with their having formed at much higher z and then subsequently passively evolved into present-day giant ellipticals (Lilly & Longair 1984, Lilly 1989, Rigler et al. 1992, Eales et al. 1996, Best et al. 1998, McCarthy 1999). Recent work has indicated that at $z \sim 2.5$ or higher, radio galaxies have more unsettled morphologies (Pentericci et al. 1999, van Breugel et al. 1999), and there is a larger spread in absolute magnitude (Lacy et al. 2000), indicating that at $z \sim 3 - 5$ we may be reaching the epoch of radio galaxy formation. Much less is known about the evolution of the population of the hosts of radio-loud quasars, but the available data paint a broadly similar picture (e.g. Lehnert et al. 1992, 1999; Ridgway & Stockton 1997; McLure et al. 1999).

While the most powerful radio galaxies are extremely rare objects, the lower-luminosity radio sources have much higher space densities. For H$_0$ = 50 km s^{-1} Mpc^{-1} and $\Omega = 1$, 3CR radio galaxies at $z = 2.5$ have a co-moving space density of only 0.2 Gpc$^{-3}\Delta$logP_{rad}^{-1} while the fainter 6C (Eales et al. 1997), 7C (Lacy et al. 1999; Willott 2000), and MRC (McCarthy et al. 1996) radio galaxies have space densities roughly $10^2 - 10^3$ times larger (Dunlop & Peacock 1990). These values can be compared to the present-day space-density of first-ranked cluster galaxies (roughly 5000 Gpc^{-3}, Bahcall & Cen 1993). Allowing for a short lifetime for the radio galaxy phase, the evolved

descendants of radio sources over a range in luminosities would account for a modest fraction of the first-ranked cluster elliptical galaxies.

In contrast, however, radio-quiet quasars of the luminosity we have studied in this paper are far more common, and therefore are more plausible progenitors of typical present-day early-type galaxies. Radio-quiet quasars with $M_B \leq -23$ have co-moving space densities at z~2 of ~2×10^4 Gpc^{-3} (Hartwick & Schade 1990). Now, for a quasar lifetime on the order of the Eddington growth-time (a few % of the Hubble time at z = 2), the implied space density of the present-day descendants is about 10^6 Gpc^{-3}, which is comparable to the space density of L_* E's and S0's (e.g. Fukugita, Hogan, & Peebles 1998). This identification is quite consistent with the correlation between the masses of supermassive black holes and the spheroids in which they live today. A quasar with $M_B = -24$ powered by accretion at the Eddington rate requires $M_{BH} \sim 2 \times 10^8$ $M_\odot$, and this supermassive black hole would live today in a spheroid with a mass of about 5×10^{10} $M_\odot$ and a V-band luminosity of about 1.5×10^{10} $L_\odot \sim 0.4$ L_*.

Though inconsistent with passive evolution like that observed in the radio galaxies, our finding L_* hosts at $z \sim 2$ – 3 (and the similar results reported by Rix et al. [1999]) are reassuring for standard hierarchical models. The types of quasar hosts we have imaged can easily be the precursors of typical present-day bulge-dominated L_* galaxies, provided that they continue to grow somewhat through mergers from $z \sim 2$ to 3 until the present day. Our typical high-z host might need to accrete a factor of few in mass in order to reach the magnitude of a $z = 0$ L_* galaxy.

Indeed, these results agree fairly well with the specific predictions of the hierarchical galaxy formation models of Kauffmann & Haehnelt (2000), in which they have addressed both the formation of bulges and the formation and fuelling of their associated black holes. They predict median host luminosities that are somewhat below present-day L_* for quasars at $z = 2$ (and even fainter at $z = 3$), for quasars with the nuclear magnitudes of our sample. In Figure 13 we show our data superimposed on their models. Our galaxies span the range of their model results, though our average host is brighter than the average of the model galaxies shown. In their model, these hosts are still undergoing major mergers which would allow them to evolve into the present day L_* or several L_* galaxies. These models are also able to reproduce the tight correlation of bulge velocity dispersion to black hole mass (Haehnelt & Kauffmann 2000).

As the typical quasar lifetime is probably short, in observing active quasars we may be selecting quite different samples of objects at $z \sim 2$ – 3, the peak of the quasar number density, from those at low-z. At low-z, where the number density of quasars has decreased dramatically, the hosts of most quasars are rarer and somewhat more massive than the more common L_* galaxies that are the possible descendants of our high-z quasar hosts. These high z hosts may evolve therefore into more common, less active low-z counterparts, such as Seyferts and quiescent L_* spheroids. This would make their evolution similar to those of the field ellipticals and Lyman break galaxies, (Dickinson et al. 1999; Steidel et al. 1999), whereas the most massive galaxies like the radio galaxies will undergo a very different evolution, associated with an early formation epoch.

6.4.2. *Relation to the Lyman break galaxy population*

The co-moving space density of the Lyman break galaxies (near the turnover of their UV luminosity function) is roughly 10^6 Gpc^{-3} (e.g. Dickinson 1998). If the hosts of radio-quiet quasars are drawn from the Lyman break population, then we conclude that only a few percent of these galaxies need host a radio-quiet quasar at any given time. If there is a population of unbeamed ("type 2") quasars at high-z (analogous to the Seyfert 2 galaxies at low-z) then the total fraction of the Lyman break galaxies hosting an AGN might be several times larger. These relative numbers are consistent with a simple model in which the lifetime of the Lyman break phase (high star-formation rates) is roughly 10^9 years (cf. Ferguson, Dickinson, & Williams 2000) and the AGN phase is roughly 10^8 years (comparable to the characteristic Eddington growth time).

Could a significant fraction (a few percent) of the known Lyman break population population be the "quasar 2's"? By hypothesis, these would be objects in which the quasar is hidden from direct view along our line-of-sight. By analogy to Seyfert 2 galaxies in the local universe (e.g. Heckman et al. 1997; Gonzalez Delgado, Heckman & Leitherer 2000) the rest-frame UV light in these galaxies would be dominated by light from young stars, and so these could naturally enter the color-selected Lyman break samples. If they are like local type 2 Seyferts, they could be distinguished from the majority of "normal" Lyman break galaxies because they would show relatively strong but rather narrow ($\leq 10^3$ km s^{-1}) nebular emission-lines. The Lyα line would normally be the strongest, but lines from highly ionized species like HeII λ1640, CIV λ1550, and NV λ1240 should also be present with strengths of roughly 5 to 20% of Lyα. This picture appears to be quite consistent with the spectroscopic properties of the Lyman break galaxies. C. Steidel (private communication) finds that $\sim$ 1.5% of spectroscopically confirmed Lyman break galaxies at z~3 are obvious narrow-lined AGNs with Seyfert-2-like spectra. This is a lower bound to the actual fraction, since the weak NV, CIV, and HeII lines could be missed in many other cases.

An obvious way to test the similarity between the Lyman break galaxies and the hosts of high-redshift AGN would be to obtain rest-frame UV images of the quasar hosts in the present sample. Our on-going HST WFPC2 imaging program will make this test possible.

7. SUMMARY

We have reported the results of the analysis of HST NICMOS images of 5 faint ($M_B \sim -23$) radio-quiet quasars at redshifts ($z \sim 2$ to 3) near the peak of the quasar epoch in the early universe. Our work complements the analysis reported by Rix et al. (1999) of six luminous ($M_B \sim -26$) gravitationally-lensed radio-quiet quasars at similar redshifts.

While the samples are still modest in size, several conclusions can already be drawn:

- Typical radio-quiet quasars at $z \sim 2$ to 3 are hosted by galaxies with rest-frame absolute visual

magnitudes similar to present-day L_* galaxies (M_V = -20 to $-23 \equiv M_{*,V} \pm 1.5$ mag).

- As such, they are much fainter than radio galaxies at the same redshift (typically by ~ 2 magnitudes).

- These host galaxies are comparable to or less luminous than the hosts of similarly-powerful low-z radio-quiet quasars. Since the luminosity-weighted mean age of the stellar population in the high-z hosts is almost certainly younger than that of the low-z hosts, the difference in stellar *mass* will be even more pronounced, by perhaps a factor of 6. The high-z hosts are also more compact than the low-z hosts (half-light radii typically <4 kpc *vs.* 8 kpc).

- The rest-frame-visual luminosities and sizes of the radio-quiet quasar hosts are roughly similar to those of the Lyman-break galaxies at similar redshifts. Thus, the Lyman-break population could represent the parent population of typical radio-quiet quasars. Our Cycle 8 HST WFPC2 observing program will determine whether this similarity extends into the rest-frame UV.

The potential implications of these results are quite significant. First, they imply that the well-studied cosmic evolution of the hosts of the very radio-loud AGN population (radio galaxies and radio-loud quasars) is evidently not representative of the much more numerous radio-quiet population. Second, by assuming either that the ratio of L_Q/M_{BH} is roughly independent of redshift or that $M_{BH} \propto M_{bulge,z=0}$, it follows that these quasars are associated with black holes with masses of about 10^8 M$_\odot$. Therefore, supermassive black holes must form before their host galaxies are fully assembled. This agrees qualitatively with the idea of the hierarchical assembly of massive galaxies at late epochs. Indeed, as already pointed out by Rix et al. (1999) and Ridgway et al. (1999), the observations agree well with the recent theoretical predictions of Kauffmann & Haehnelt (2000). We might expect that the average low-z counterparts of these high-z quasar hosts may be quiescent bulge-dominated systems rather than the massive galaxies associated with the low-z active quasar population.

REFERENCES

Aretxaga, I., , Boyle, B. J. & Terlevich, R.J. 1995, MNRAS, 275, L27.

Aretxaga, I., Le Mignant, D.; Melnick, J., Terlevich, R. J., Boyle, B.J. 1998, MNRAS, 298, 13

Bahcall, N.A. & Cen, R. 1993, ApJ, 407, 49.

Bahcall, J., Kirhakos, S., Saxe, D., & Schneider, D. 1997, ApJ, 479, 642

Best, P. N., Longair, M. S., Röttgering, H. J. 1998, MNRAS, 295, 549

Bruzual, G. & Charlot, S. 1993, ApJ, 405, 538.

Bruzual, G. & Charlot, S. 2000, in preparation.

Dickinson, M. 2000, Philosophical Transactions of the Royal Society, Series A.

Dickinson et al. 2000, in preparation.

Dunlop, J.S. 1998, in *Observational Cosmology with the New Radio Surveys*, Proceedings of a Workshop held in Puerto de la Cruz, Tenerife, Canary Islands, Spain, 13-15 January 1997, Dordrecht: Kluwer Academic Publishers

Eales, S., Rawlings, S., Law-Green, D., Cotter, G., & Lacy, M. 1997, MNRAS, 291, 593

Elvis, M. et al. 1994, ApJS, 95, 1

Ferguson, H. C., Dickinson, M., & Williams, R. 2000, to appear in ARA&A, vol. 38, (astro-ph/0004319).

Ferrarese, L. & Merrit, D. 2000, ApJL, submitted, astro-ph/0006053.

Fukugita, M., Hogan, C. J., Peebles, P. J. E. 1998, ApJ, 503, 518.

Gebhardt, K. et al. 2000a, astro-ph/0006289.

Gebhardt, K. et al. 2000b, astro-ph/0007123.

Haehnelt, M.G. & Kauffmann, G. 2000, MNRAS, submitted, astro-ph/0007369.

Giavalisco, M., Steidel, C. C., Macchetto, F. D. 1996, ApJ, 470, 189.

Gonzalez-Delgado, R.M., Heckman, T., & Leitherer, C. 2000, Proceedings of the JENAM Conference (Toulouse, September 1999). To be published in EDPS Conference Series in å, Eds. B. Rocca-Volmerange and H. Sol (astro-ph/0001104).

Hartwick, F.D. & Schade, D. 1990, ARA & A, 28, 437.

Heckman, T. M., Gonzalez-Delgado, R., Leitherer, C., Meurer, G. R., Krolik, J., Wilson, A. S., Koratkar, A. and Kinney, A. 1997, ApJ, 482, 114.

Hooper E.J., Impey C.D., Foltz C.B., 1997, ApJ, 480, L95

Kauffmann, G., & Haehnelt, M. 2000, MNRAS, 311, 576

Kormendy J., Richstone D., 1995, ARA&A, 33, 581

Kukula, M. J., et al. 2000, astro-ph/0010007.

Lacy, M., Rawlings, S., Hill, G. J., Bunker, A. J., Ridgway, S.E., Stern, D. 1999, MNRAS, 308, 1096.

Lacy, M., Ridgway, S., & Trentham, N. 1999, To appear in "Lifecycles of Radio Galaxies", eds. J. Biretta et al., New Astronomy Reviews (astro-ph/9909163).

Lacy, M., Bunker, A., Ridgway, S. E. 2000, AJ, 120, 68.

Laor, A. 1998, ApJL, 505, L83

Lehnert, M. D., Heckman, T. M., Chambers, K. C., Miley, G. K. 1992, ApJ, 393, 68.

Lehnert, M. D. et al. 1999, ApJS, 123, 351

Lilly, S.J. & Longair, M.S. 1984, MNRAS, 211, 833

Lilly, S. J. 1989, ApJ, 340, 77.

Liu, M.C., Charlot, S., & Graham, J. R. 2000, ApJ, in press (astro-ph/0004367).

Loveday, J., Peterson, B., Efstathiou, G., Maddox, S. 1992, ApJ, 390,338.

Lowenthal, J. D., Heckman, T. M., Lehnert, M.D., & Elias, J.H. 1995, ApJ, 439, 588.

Lowenthal, J.D. et al. 1997, ApJ, 481, 673.

Magorrian J., et al., 1998, AJ, 115, 2285

Marano, B., Zamorani, G., & Zitelli, V. 1988, MNRAS, 232, 111.

McCarthy, P.J., Kapahi, V. K., van Breugel, W., Persson, S. E., Athreya, R., Subrahmanya, C. R. 1996, ApJS, 107, 19.

McLure, R. J., Kukula, M. J., Dunlop, J. S., Baum, S. A., O'Dea, C. P. & Hughes, D. H. 1999, MNRAS, 308, 377

McLure, R.J. & Dunlop, J.S. 1999, MNRAS, submitted (astro-ph/9908214).

McLeod, K. & Rieke, G. 1995, ApJ, 454, L77

McLeod, K., Rieke, G., & Storrie-Lombardi, L. 1999, ApJL, 511, L67

Najita, J., Dickinson, M., Holfeltz, S. 1998, NICMOS Instrument Science Report ISR-98-001.

Pentericci, L., Röttgering, H.J., Miley, G.K., McCarthy, P., Spinrad, H., van Breugel, W. & Macchetto, F. 1999, A & A, 341, 329.

Pentericci, L., McCarthy, P.J., Miley, G.K., Röttgering, H.J., & van Breugel, W. 2000, ApJ, submitted.

Pentericci, L. PhD Thesis.

Ridgway, S.E., & Stockton, A. 1997, ApJ, 114, 511.

Ridgway, S. E., Heckman, T., Calzetti, D. & Lehnert, M., 1999, To appear in *Lifecycles of Radio Galaxies*, eds. J. Biretta et al., New Astronomy Reviews (astro-ph/9911049).

Rix, H.-W. et al. 1999, to appear in *Gravitational Lensing: Recent Progress and Future Goals*, eds. T. Brainerd and C. Kochanek [astro-ph/9910190]

Rigler, M.A., Lilly, S.J., Stockton, A., Hammer, F., & LeFèvre, O. 1992, ApJ, 385, 61

Roche, N., Eales, S. & Rawlings, S. 1998, MNRAS, 297, 405.

Röttgering, H. J. A., Best, P. N. and Lehnert, M. D. 1999, "The Most Distant Radio Galaxies", Proceedings of the Colloquium, Amsterdam, 15-17 October 1997, Royal Netherlands Academy of Arts and Sciences. Eds. H. J. A. Röttgering, P. N. Best and M. D. Lehnert.

Skinner, C.J. et al. 1998, Proc. SPIE, vol. 3354, p. 2

Steidel, C., Adelberger, K., Giavalisco, M., Dickinson, M., & Pettini, M. 1999, ApJ, 519, 1

Terlevich R., Boyle B.J., 1993, MNRAS, 262, 491

van der Marel R.P., 1999, AJ, 117, 744

van Breugel, W., de Breuck, C., Stanford, S.A., Stern, D., Röttgering, H., Miley, G. 1999, ApJ, 518, 61.

Wandel, A., Peterson, B.M., Malkan, M.A. 1999, ApJ, 526, 579.

Willott, C. 2000, PhD thesis.

Zitelli, V., Mignoli, M.; Zamorani, G.; Marano, B.; Boyle, B. J., 1992, MNRAS, 256, 349

TABLE 1

PROPERTIES OF SAMPLE AND OBSERVATIONAL LOG

Name	RA J2000	DEC J2000	Redshift	B (Nuclear)	Filter	λ_0[a] (Å)	Exposure Time (seconds)	$\sigma_{\rm sky}$[b] (μJy arcsec^{-2})
MZZ 9744	03 13 38.33	-55 21 37.0	2.735	21.9	F160W	4284	11007	0.48
MZZ 9592	03 14 04.94	-55 20 50.9	2.710	21.9	F160W	4312	12543	0.48
MZZ 1558	03 14 51.48	-54 57 14.5	1.829	21.6	F165M	5832	9919	0.97
MZZ 11408	03 15 34.10	-55 30 04.8	1.735	22.0	F165M	6033	9983	1.10
MZZ 4935	03 16 36.25	-55 09 32.2	1.876	21.9	F165M	5737	18943	0.75

[a]Mean rest wavelength of observation.

[b]1σ scatter per pixel in surface brightness from sky noise (1 pixel = 0$''$0375).

TABLE 2

HOST GALAXY PHOTOMETRY

Name	Redshift	M_B (Nucleus)	Aperture radius	H Host flux (μJy)	$M_{\rm host}$	Host luminosity	Total $M_{\rm host}$[a]
MZZ 9744	2.735	-23.8	0$''$64	1.08 ± 0.4	-21.3 (B) $\pm$ 0.5	1.3 L_*^B	
$\cdots$	$\cdots$	$\cdots$	1$''$01	1.32 ± 0.4	-21.5 (B) $\pm$ 0.5	1.6 L_*^B	-21.8 (B)
MZZ 9592	2.710	-24.2	0$''$64	3.21 ± 0.2	-22.5 (B) $\pm$ 0.1	3.9 L_*^B	
$\cdots$	$\cdots$	$\cdots$	1$''$01	3.37 ± 0.2	-22.5 (B) $\pm$ 0.1	4.0 L_*^B	-22.9 (B)
MZZ 1558	1.829	-23.8	0$''$64	$2.44^{+0.4}_{-0.5}$	-21.6 (V) $\pm$ 0.2	0.8 L_*^V	
$\cdots$	$\cdots$	$\cdots$	1$''$01	3.27 ± 0.5	-21.9 (V) $\pm$ 0.2	1.1 L_*^V	-22.5 (V)
MZZ 11408	1.735	-21.9	0$''$64	$2.63^{+0.3}_{-0.7}$	-21.5 (V) $^{-0.3}_{+0.4}$	0.8 L_*^V	
$\cdots$	$\cdots$	$\cdots$	1$''$01	$3.12^{+0.3}_{-0.7}$	-21.7 (V) $^{-0.3}_{+0.4}$	0.9 L_*^V	-22.0 (V)
MZZ 4935	1.876	-22.0	0$''$64	0.58 ± 0.2	-20.1 (V) ±0.4	0.2 L_*^V	
$\cdots$	$\cdots$	$\cdots$	1$''$01	1.01 ± 0.2	-20.2 (V) ±0.4	0.2 L_*^V	-20.6 (V)

[a]This approximate "total" magnitude is estimated from the measured $M_{\rm host}$ within 2$''$ by adding the appropriate subtraction corrections from the HDF LBG models (Table 5) and the aperture corrections given in Table 3.

TABLE 3

QUASAR HOST SCALE SIZES

Name	Redshift	$r_{\frac{1}{2}}$[a]	model type:$r_{\frac{1}{2}}$[b]	Aperture Correction[c] (Δ mags)
(1)	(2)	(3)	(4)	(5)
MZZ 9744	2.735	0$''$24	$\cdots$	0.1
MZZ 9592	2.710	0$''$31	disk: 0$''$26 $-$ 0$''$31	0.1
$\cdots$	$\cdots$	$\cdots$	bulge: 0$''$11 $-$ 0$''$18	$\cdots$
MZZ 1558	1.829	0$''$39	$\cdots$	0.3
MZZ 11408	1.735	0$''$25	disk: 0$''$24 $-$ 0$''$22	0.2
$\cdots$	$\cdots$	$\cdots$	bulge: 0$''$14 $-$ 0$''$37	$\cdots$
MZZ 4935	1.876	0$''$25	$\cdots$	0.2

[a]Half-light radius determined directly from enclosed flux profile of PSF-subtracted residual host. This determination assumes the inner 0$''$2 is flat.

[b]Range of $r_{\frac{1}{2}}$ determined by fitting (where possible) disk and bulge profiles to the 1D radial profile of the subtracted host.

[c]Change in magnitude due to flux excluded from a 2$''$ aperture, for a host galaxy with the given $r_{\frac{1}{2}}$.

TABLE 4
QUASAR NUCLEAR PROPERTIES

Name	Redshift	Nuclear Flux(H)[a] (μJy)	M_B(Nucleus)	α[b]	Nuclear Fraction [c]
MZZ 9744	2.735	10.6 ± 0.5	−23.8	+0.6	89%
MZZ 9592	2.710	15.9 ± 0.5	−24.2	−0.6	83%
MZZ 1558	1.829	24.5 ± 0.8	−23.8	−0.7	90%
MZZ 11408	1.735	3.9 ± 0.2	−21.9	+0.2	56%
MZZ 4935	1.876	3.4 ± 0.2	−22.0	−0.3	77%

[a]Nuclear flux derived from PSF subtraction fit, includes all NICMOS PSF energy enclosed within a 5″7 aperture

[b]The spectral index α ($f_\nu \propto \nu^\alpha$), from observed B to H.

[c]Percentage of total flux due to the nucleus.

TABLE 5
SUMMARY OF MODEL RESULTS: MAGNITUDE CORRECTIONS

Model Type[a]	Model Nucleus[b]		Quasars[c]	Δ Magnitudes[d]		
(1)	H Flux(μJy) (2)	M_B[e] (3)	(4)	HDF galaxies (5)	Radio galaxies (6)	Ellipticals/Disks (7)
$z = 1.8$ low	3.7	−21.9	MZZ 4935, MZZ11408	0.13	0.33	0.11
$z = 1.8$ medium	14.5	−23.4	—	0.25	0.32	0.14
$z = 1.8$ high	25.3	−24.0	MZZ 1558	0.32	0.32	0.25
$z = 2.7$ low	5.0	−22.9	—	0.13	0.44	0.18
$z = 2.7$ medium	10.6	−23.7	MZZ 9744	0.16	0.45	0.35
$z = 2.7$ high	15.9	−24.2	MZZ 9592	0.25	0.46	0.43

Note. — Here we summarize the results of the models discussed in the text, in which we have created artificial quasars with a range of model host galaxies and a range of nuclear brightnesses, and determined how much flux was lost by the process of PSF-subtraction.

[a]The redshift of the model, and whether a nucleus of low, medium or high brightness was used.

[b]The H flux and absolute B magnitude of the nucleus for this model type.

[c]The observed quasars whose redshift and nuclear brightnesses correspond to this model type.

[d]The average flux lost, in magnitudes, for the models which use the given sample of galaxies and the given nuclear brightnesses.

[e]M_B is calculated from the H flux using spectral index $\alpha = +0.2$

TABLE 6
BLACK HOLE MASS AND ACCRETION RATE ESTIMATES

Name	Redshift	$M_{BH}/10^8 M_\odot$[a]	L_Q/L_E[b]
MZZ 9744	2.735	0.79	1.4
MZZ 9592	2.710	2.19	0.7
MZZ 1558	1.829	1.52	0.7
MZZ 11408	1.735	1.05	0.2
MZZ 4935	1.876	0.29	0.7

[a]The black hole masses derived from our total M_V(host) corrected to $z = 0$, using the van der Marel (1999) normalization of the $L_{bulge}-M_{BH}$ relation.

[b]The ratio of the quasar luminosity to the Eddington limit, assuming the black hole masses shown here.
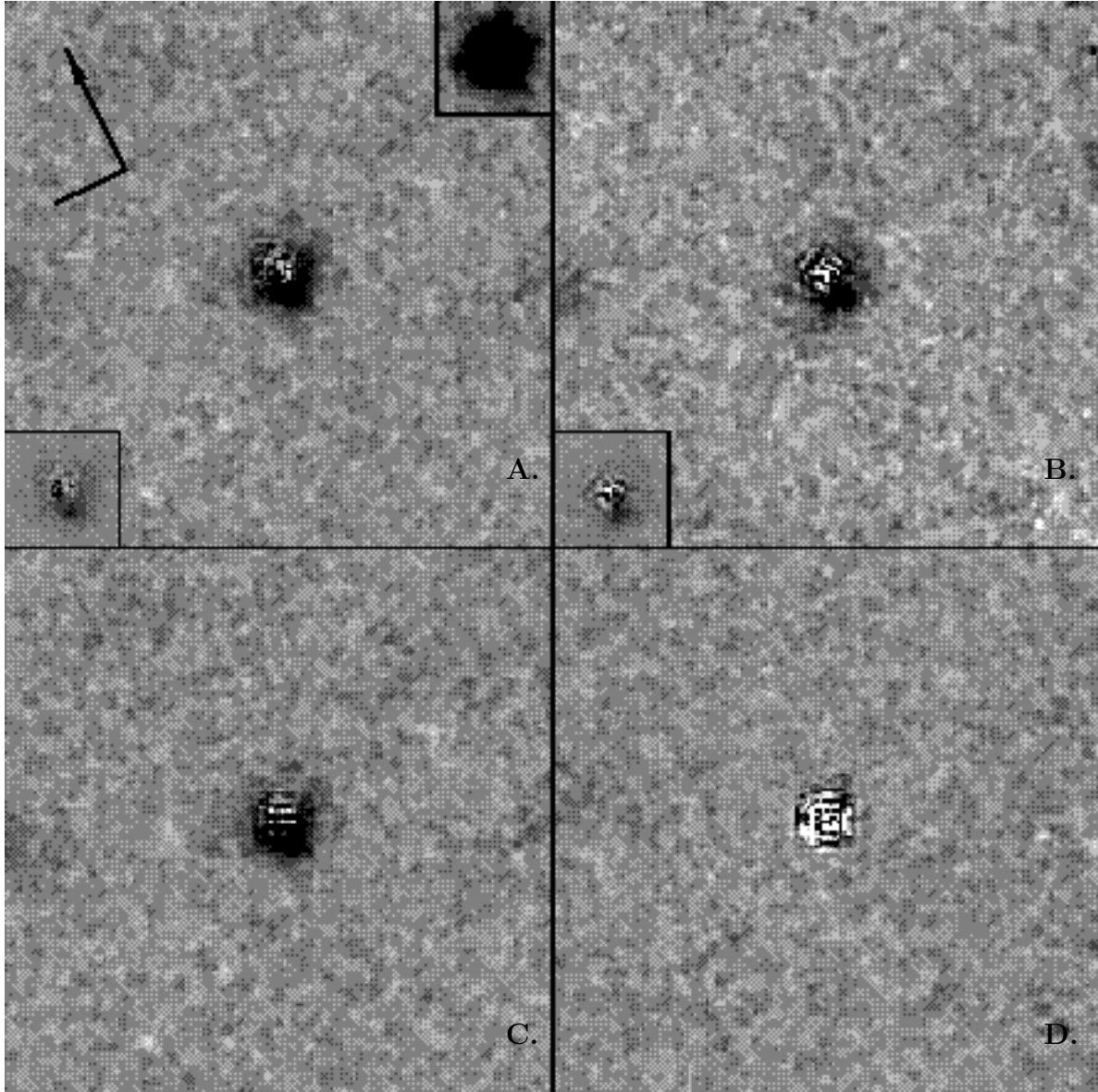
FIG. 1.— MZZ 9592, PSF subtractions and tests. All frames are $5\rlap{.}{''}7$ square; the sky position angle is indicated by the compass arrow to north. *A.* Visit one, PSF-subtracted, using the observed bright PSF star from the same visit. The central region of this same image (at a lower display stretch) is shown in the lower left inset, showing an off-center residual host component. The upper right inset shows the unsubtracted quasar. *B.* Visit two, PSF-subtracted, rotated to match the orientation of visit one. Sky noise is worse in this image, with residual low-level CR problems, but the off-nuclear component is visible (also seen in the lower left inset of the central region). *C.* Visit one, PSF-subtracted using the star that falls within the field, demonstrating that the residual is not an artifact of the mismatch between the observational strategies applied to the quasar fields and the bright PSF stars. *D.* The field star minus the PSF star: no net residual flux.

Raw   Smoothed

MZZ 11408

MZZ 1558

MZZ 4935
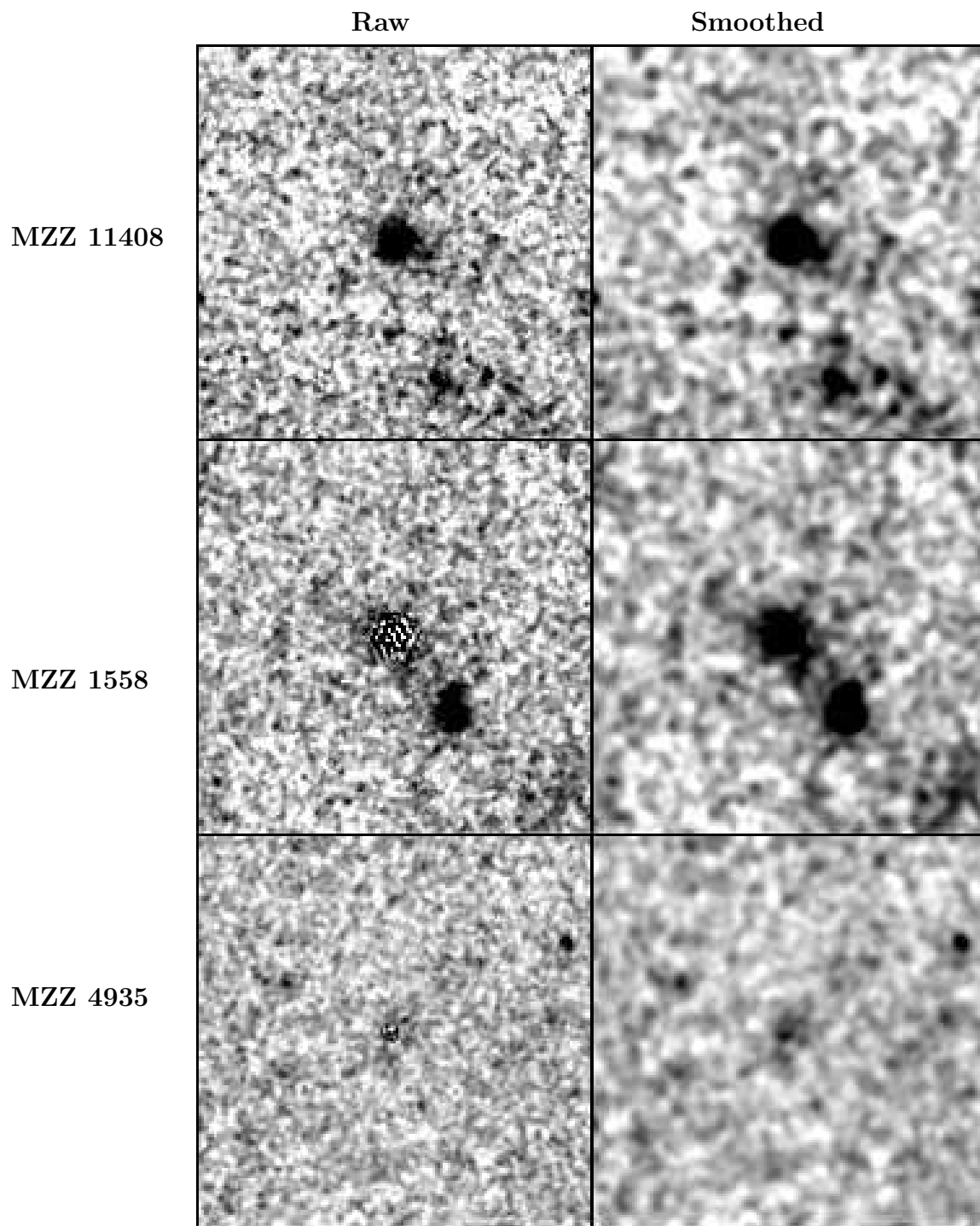
FIG. 2.— PSF-subtracted $z \sim 2$ MZZ quasar hosts. Right panels show images that are smoothed with a Gaussian kernel with $\sigma=0\farcs06$. Each panel is $5\farcs7$ square (or roughly 45 kpc), N up, E left.
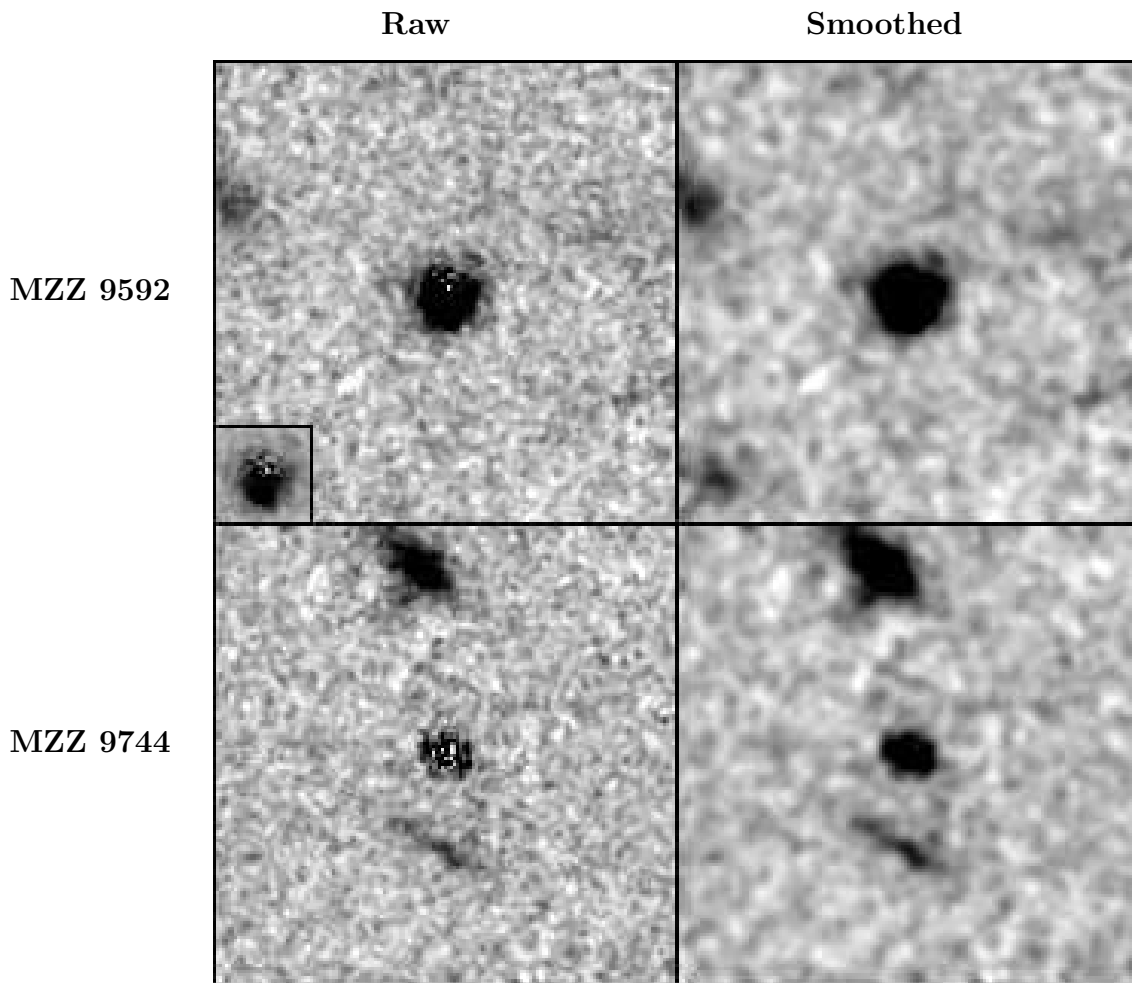
FIG. 3.— PSF-subtracted $z \sim 3$ MZZ quasar hosts, on the left unsmoothed; on the right, smoothed with a Gaussian kernel with $\sigma = 0\rlap{.}''06$. Each panel is $5\rlap{.}''7$ square (or roughly 45 kpc), N up, E left. MZZ 9592, left panel has an inset of the central region at less display stretch, showing the off-center host component.
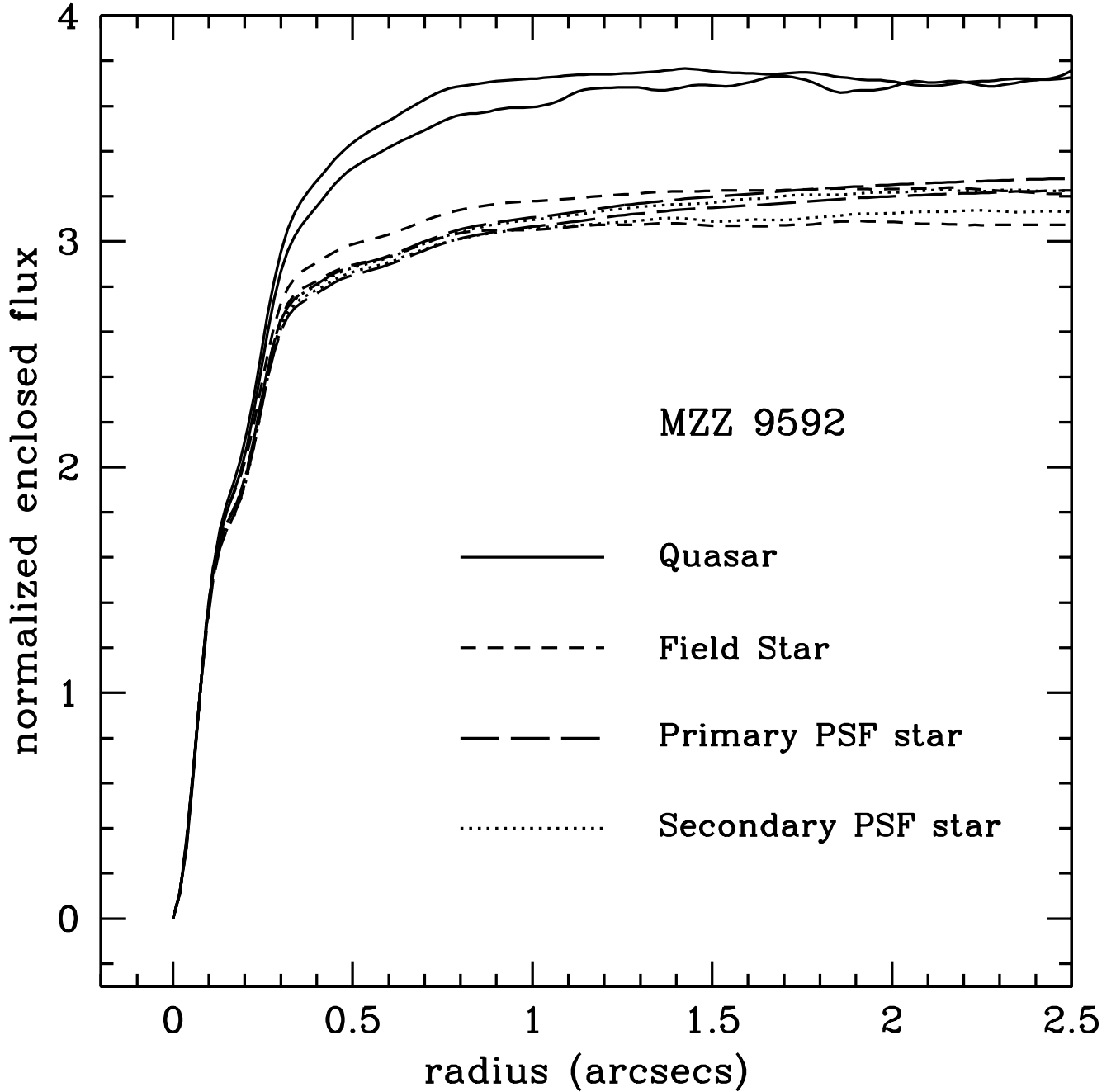
FIG. 4.— The enclosed flux is shown versus the radius of the aperture for all observations of MZZ 9592. The solid lines are the quasar in each of the two visits, while the dashed and dotted lines represent various stars observed: the field star which was observed simultaneously with the quasar, the primary PSF star, and a secondary PSF star of reasonable brightness which fell on the PSF star field. The enclosed flux has been normalized in all cases to 1 for the aperture with radius 0″075, corresponding to a diameter of ≈ 1 FWHM.
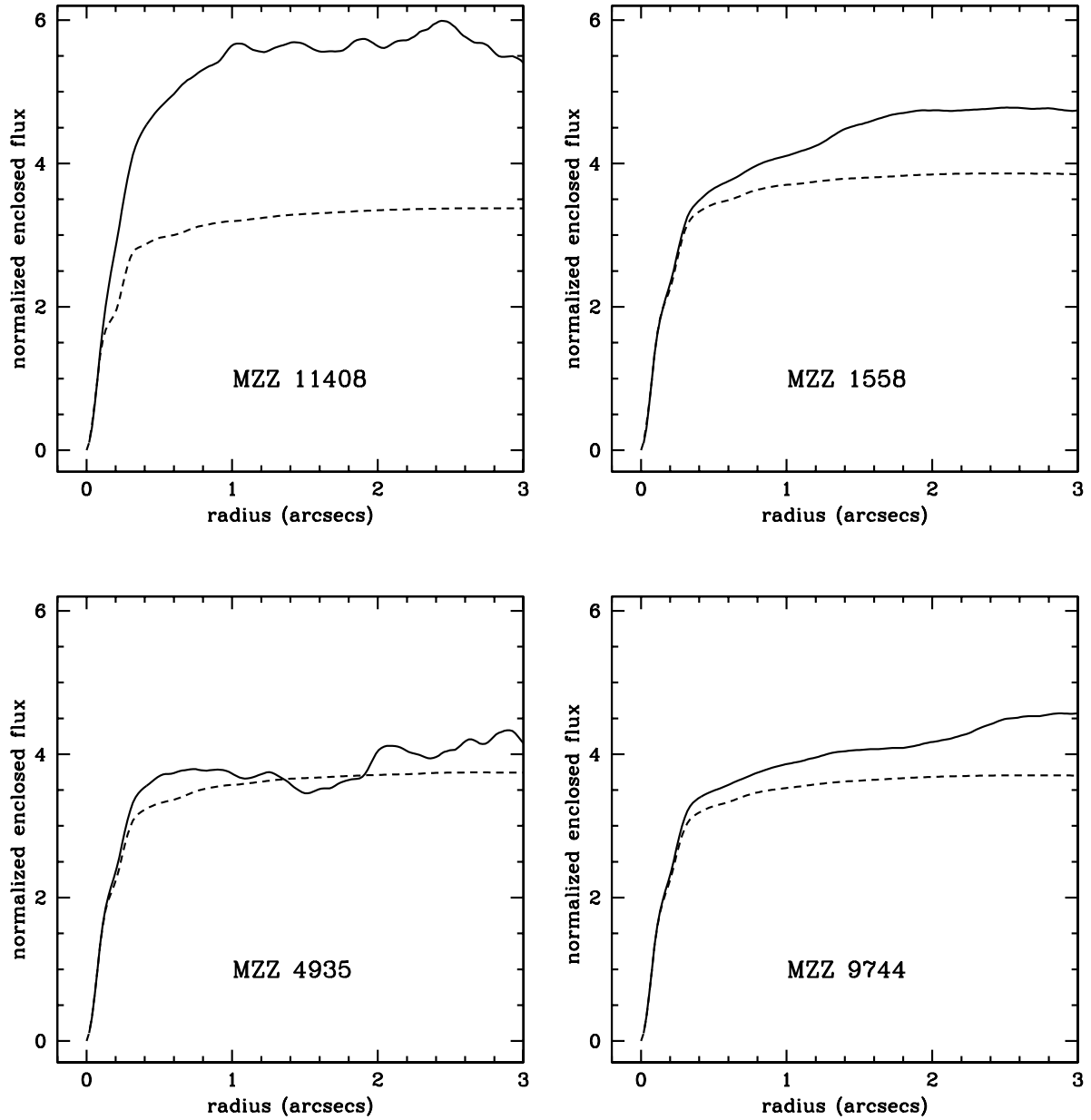
FIG. 5.— Enclosed flux plots for 4 quasars and their PSF stars. The solid line is the average of the two observations of the quasar, while the dashed line is the average of all available observations of the corresponding PSF stars. The enclosed flux values are normalized to 1 at a radius of 0.″075 as in Figure 4.
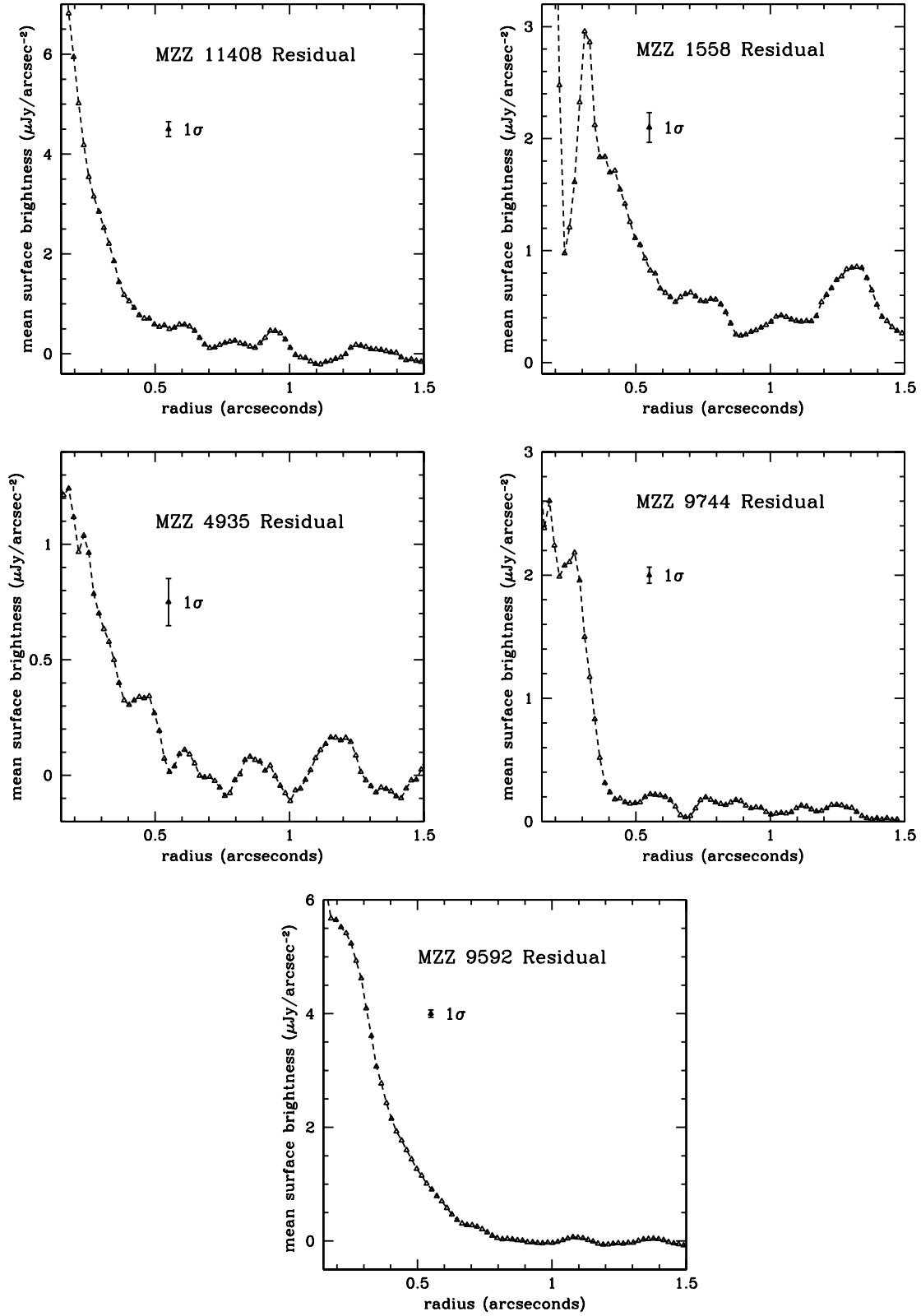
FIG. 6.— Radial profile plots of the mean surface brightness in the PSF-subtracted quasar residual extensions for which the corresponding images are shown in Figs. 2 and 3. The radial profiles are azimuthal averages made in bins of $0''.019$; in each figure we show the statistical error due to sky noise for the average bin. We do not display the inner $0''.15$ radius which is dominated by PSF residual noise in all of the quasars. The radial extent of the region in which the PSF residuals dominate varies somewhat with the brightness of the quasar nucleus.

MZZ 9592   **MZZ 11408**

Galaxy Model
Subtracted

Original
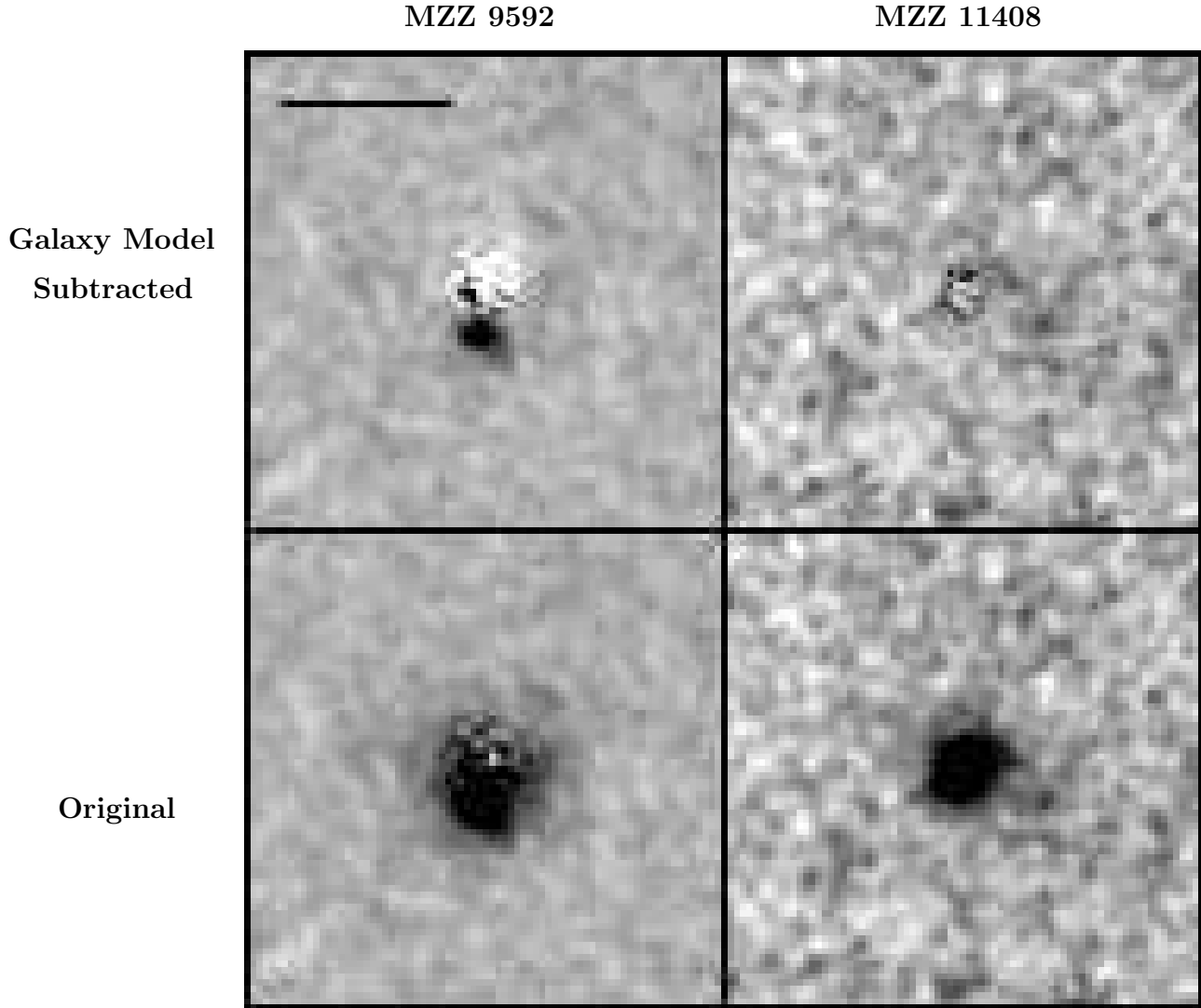
Fig. 7.— Unsmoothed images of the PSF-subtracted quasars MZZ 9592, left, and MZZ 11408, right. The bottom panels are the PSF-subtracted residual host images, while in the upper panels, a two-dimensional model of a galaxy has been subtracted as well. For MZZ 9592, this was a disk model with a $r_{\frac{1}{2}}$ of $0\overset{''}{.}25$; for MZZ 11408, this was a bulge model with $r_{\frac{1}{2}}$ of $0\overset{''}{.}3$. The black bar shows $1''$.

z = 1.8   **z = 2.7**   **z = 2.7**
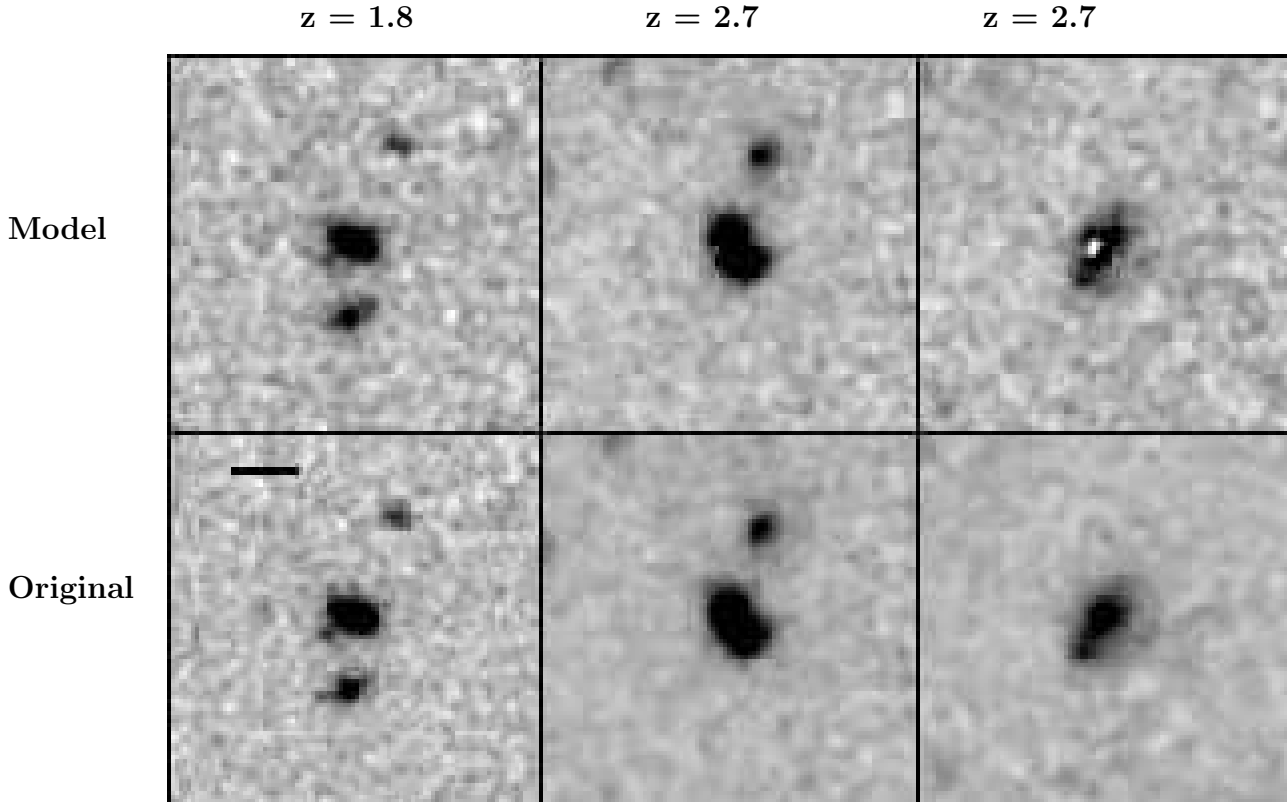
Model

Original

FIG. 8.— Examples of simulated quasars based on NICMOS-observed Lyman break galaxies: 3 HDF North galaxies from Dickinson et al. (2000), used for one $z = 1.8$ model and two $z = 2.7$ models. The bottom row shows the original galaxy before nucleus and noise is added, while the top row shows the result of adding artificial quasar nuclei, sufficient Poissonian noise to match our observed quasars, and then making a standard subtraction of an independent observed PSF. The artificial nuclei used for the models, shown from left to right, were of low, medium and high brightnesses respectively, as given in Table 5. The black bar represents $1''$, and each frame is $5.''7$. The display stretch is the same as that used in Figures 2 and 3.
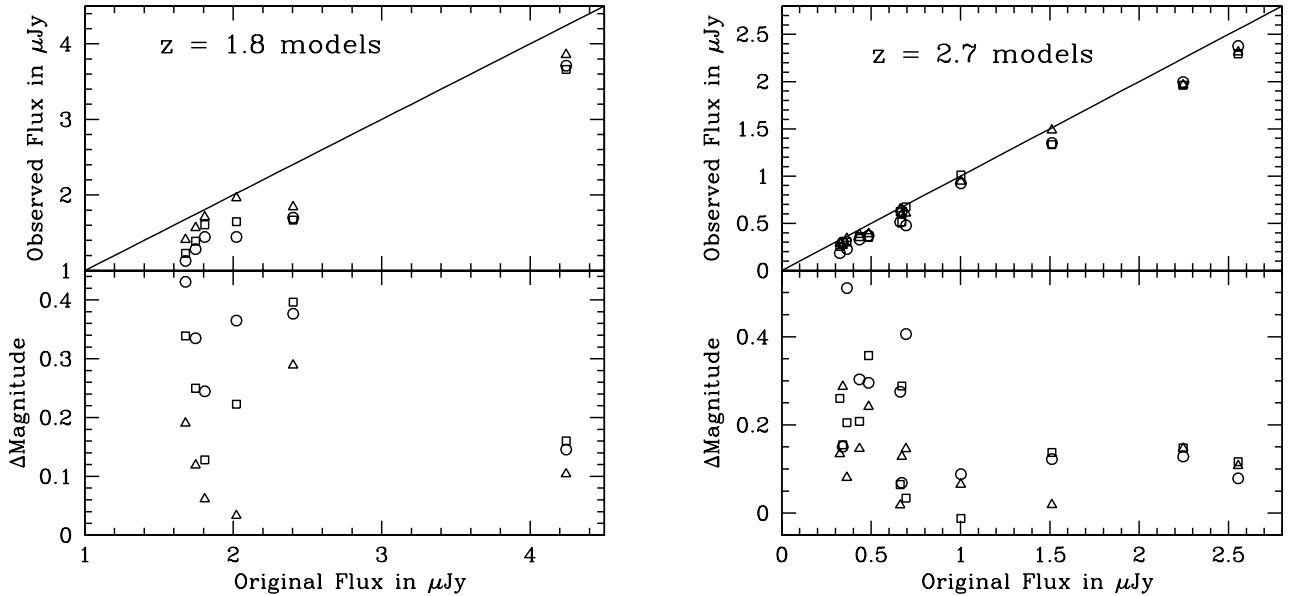

FIG. 9.— Top panels, left and right, are plots of output flux in a $1.''3$ aperture after application of our modelling and PSF-subtraction method versus the original flux in the input galaxy in the same aperture. Bottom, we give the corresponding difference in host magnitude. Each input galaxy is modelled with nuclei of three different brightnesses: the circle shows the flux from using the brightest nucleus, the square corresponds to the medium nucleus, and the triangle shows the result from using the faintest nucleus. (These model nuclear brightnesses are given in Table 5).
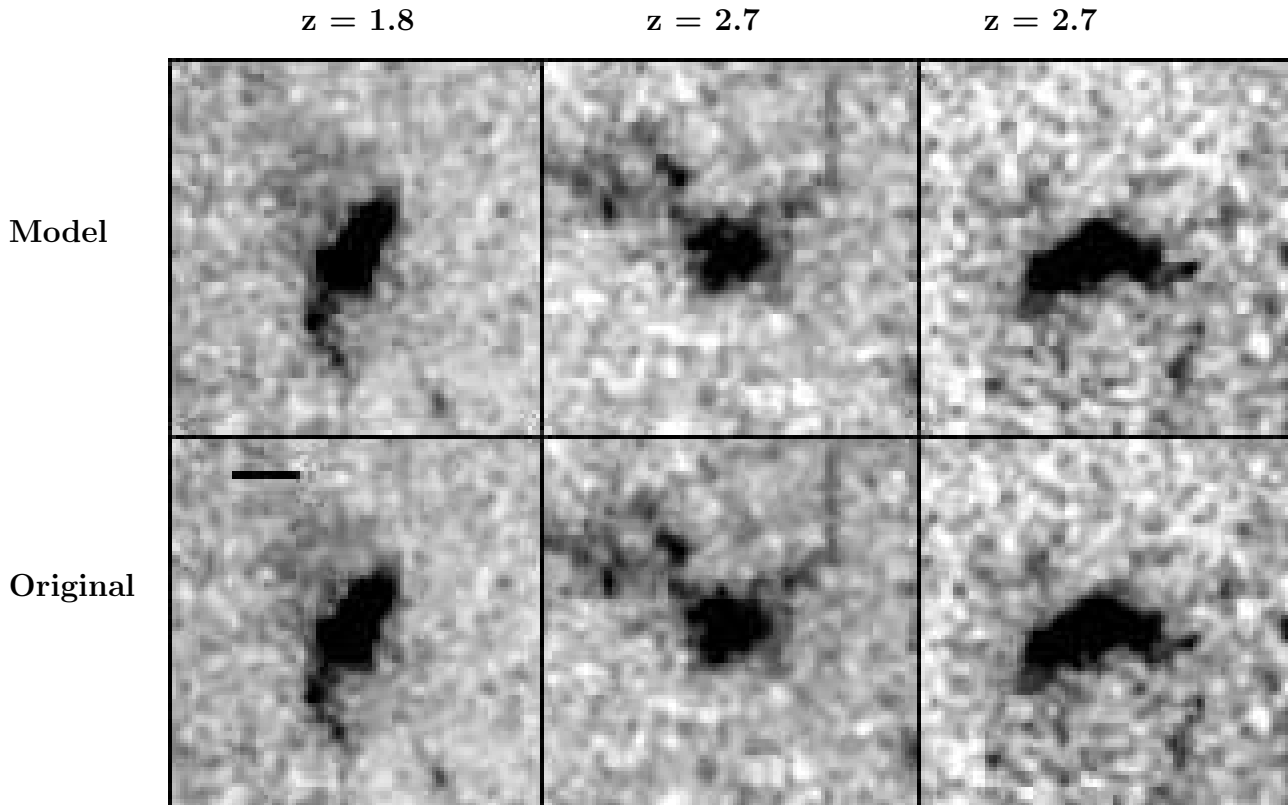
FIG. 10.— Example simulated quasars based on NICMOS-observed powerful radio galaxies: 3 MRC galaxies from Pentericci et al. 2000, used for one $z = 1.8$ model and two $z = 2.7$ models. The bottom row shows the original galaxy before nucleus and noise is added, while the top row shows the result of adding artificial quasar nuclei, sufficient Poissonian noise to match our observed quasars, and then making a standard subtraction of an independent observed PSF. The artificial nuclei used for the models, shown from left to right, were of low, medium and high brightnesses respectively, and are listed in Table 5. The black bar represents $1''$, and each frame is $5\rlap{.}''7$. The display stretch for the $z = 2.7$ images is the same as that used in Figures 2 and 3, while the $z = 1.8$ model images (at left) are shown with $10\times$ less stretch.
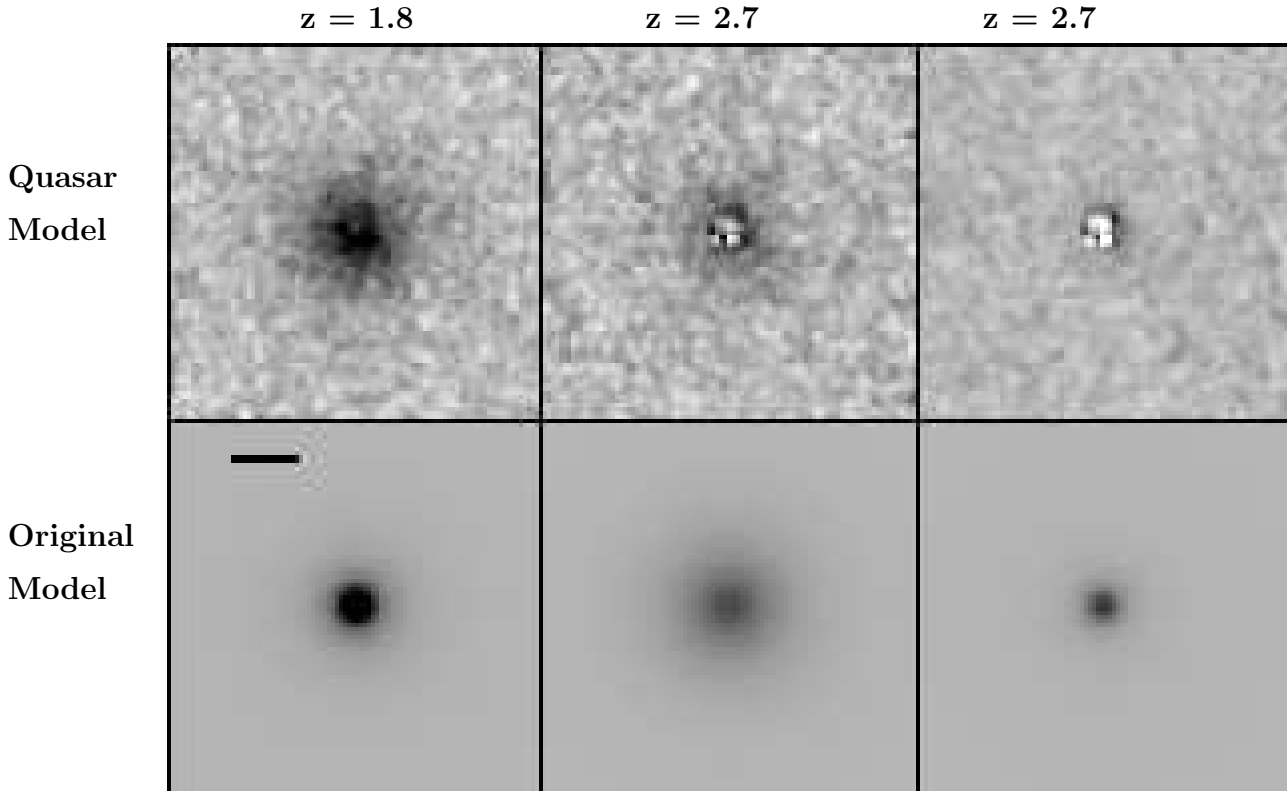
z = 1.8   **z = 2.7**   **z = 2.7**

Quasar
Model

Original
Model

FIG. 11.— Example quasars simulated from disk and elliptical models, with half-light radii of 8.2 kpc and $M_V = -22.1$: two $z = 1.8$ models and one $z = 2.7$ model. The bottom row shows the original galaxy model before nucleus and noise is added, while the top row shows the result of adding artificial quasar nuclei, sufficient Poissonian noise to match our observed quasars, and then making a standard subtraction of an independent observed PSF. The artificial nuclei used for the models, shown from left to right, were of low, medium and high brightnesses respectively. These values are given in Table 5. The galaxy model types used were elliptical, disk, and elliptical models from left to right. The black bar represents $1''$, and each frame is $5''.7$. The display stretch is the same as that used in Figures 2 and 3.
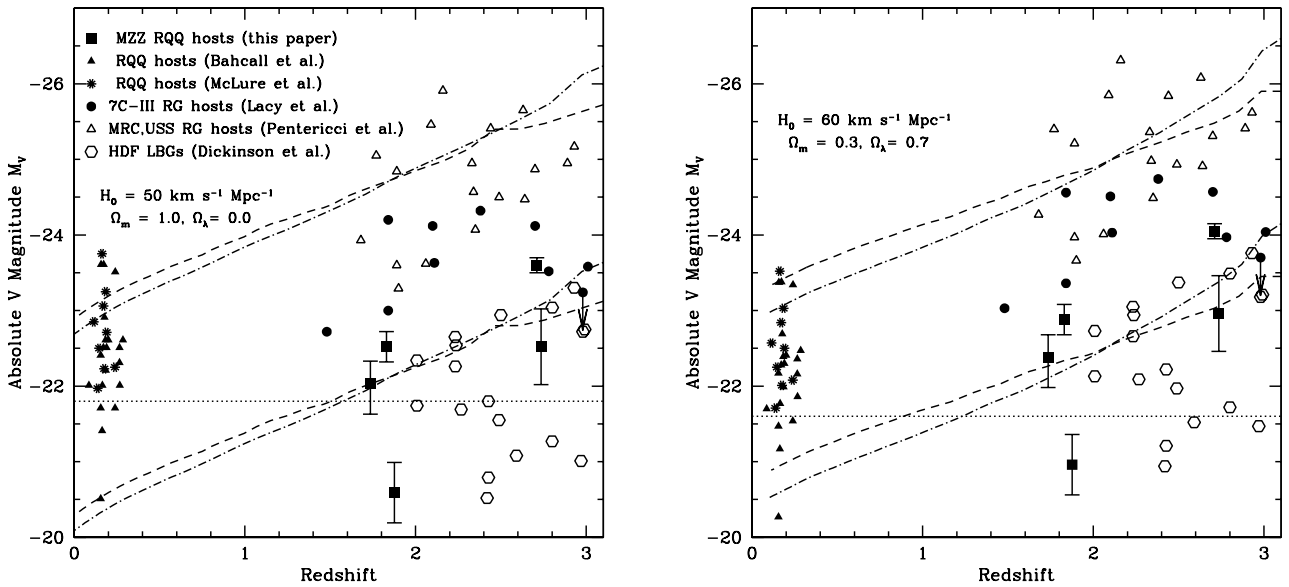

FIG. 12.— The absolute rest-frame V magnitudes versus redshift in two cosmologies for our quasar hosts (squares) and other samples of host galaxies: the low-z quasar samples of Bahcall et al. (filled triangles) and McLure et al. (stars), the 7C radio galaxy sample of Lacy et al. (filled circles), and the powerful MRC and USS radio galaxy sample from Pentericci et al. (unfilled triangles). All magnitudes are total magnitudes. The horizontal dotted line indicates present-day L$_*$. The dashed line represents the passive evolution of a model galaxy formed in an instantaneous burst of star formation at $z = 5$, while the dot-dashed line represents a model with a 1 Gyr burst of star formation ending at $z = 3$. These Bruzual & Charlot (2000) models have been generated with a Salpeter IMF and an upper mass cutoff of 100 M$_\odot$. The lower tracks for the instantaneous burst are normalized to a total mass of 1.1×10^{11} M$_\odot$ (Ω_m=1) or 2.0×10^{11} M$_\odot$ ($\Omega_m = 0.3$). The upper tracks are normalized to a total mass of 1.2×10^{12} M$_\odot$ (Ω_m=1) and 1.9×10^{12} M$_\odot$ ($\Omega_m = 0.3$).
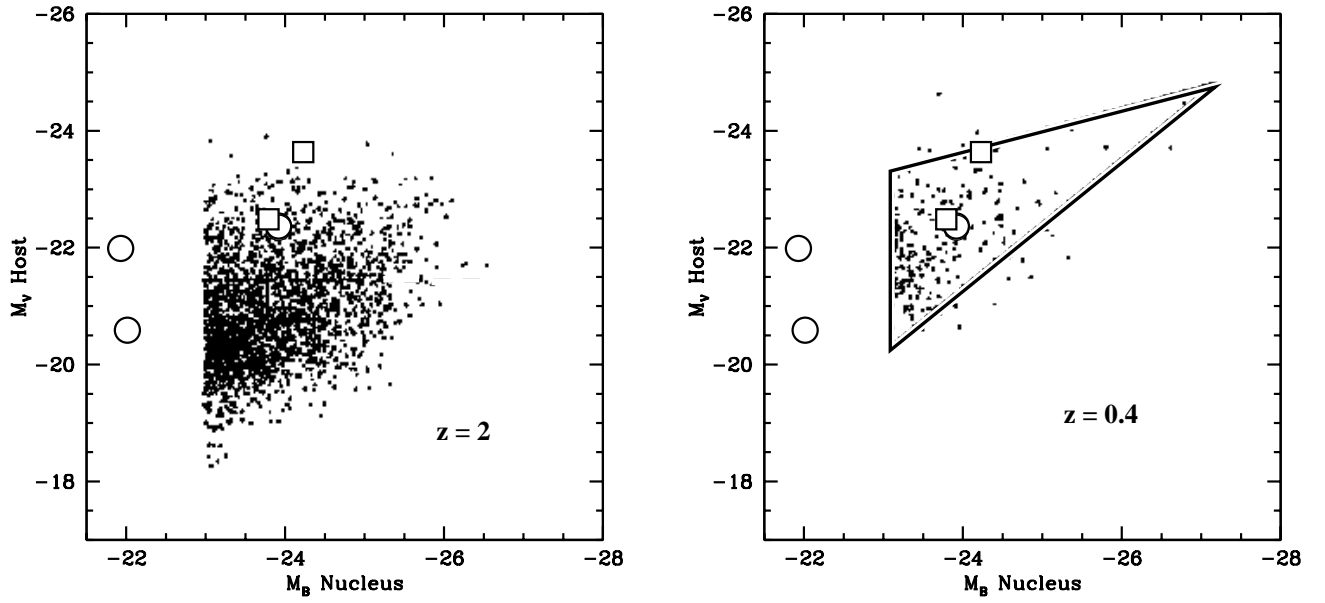
FIG. 13.— Results for the MZZ host galaxy magnitudes plotted as large unfilled symbols over the theoretical predictions (black dots) from Kauffmann & Haehnelt (2000) (adopted from their figure 12). The squares are our $z \sim 2.7$ quasar hosts, the circles are the $z \sim 1.8$ quasars, placed on both the low-z and $z \sim 2$ planes. The triangular region encompasses the low-z quasar hosts of McLeod et al. (1999).